

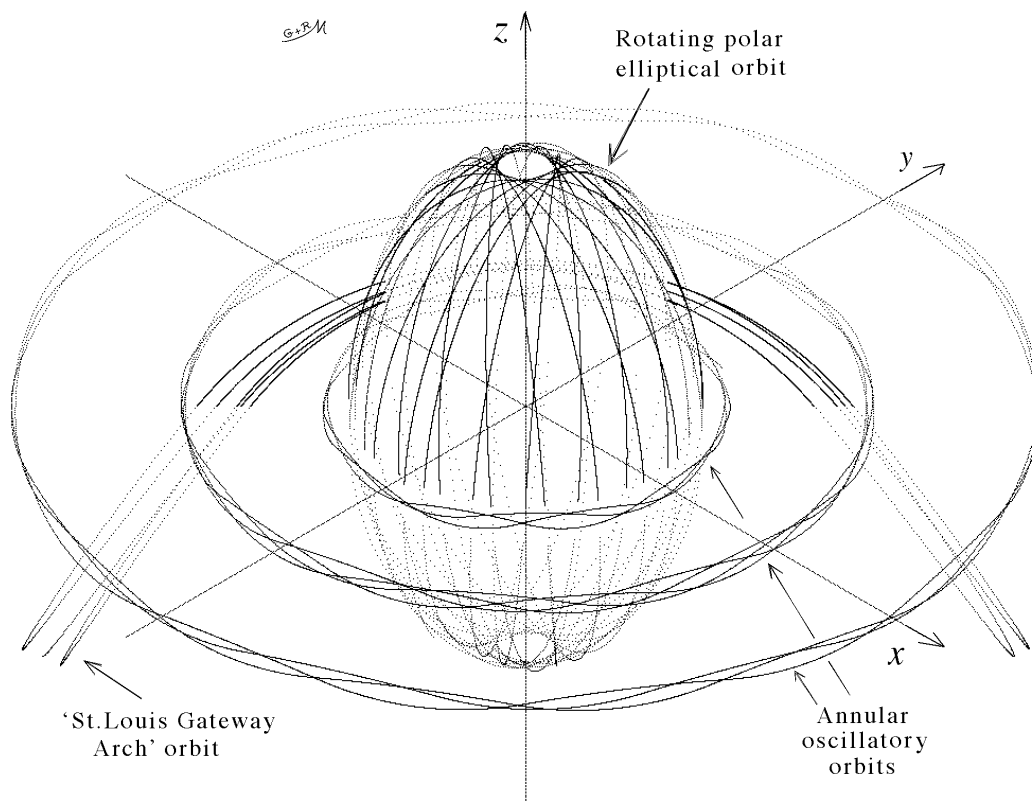
# Some Orbital and Other Properties of the ‘Special Gravitating Annulus’

Guy Moore MA PhD & Richard Moore PhD DFA FRSA

Isle of Wight, England

e-mail: math.physics.philosophy@googlemail.com

## 1. Preview Picture



**Preview picture:** A composite of independent orbits computed in isometric projection. The annular plane is the  $x,y$  plane.

(Note: As an aid to visualization, fewer of the computed orbital points are marked below the annular plane, inside the rotating elliptical polar orbits, and towards the ‘back’ of this picture.)

## 2. Abstract

Our obtaining the analytical equations for the gravitation of a particular type of mathematical annulus, which we called a ‘Special Gravitating Annulus’ (SGA), greatly facilitates studying its orbital properties by computer programming. This includes isomorphism, periodic and chaotic polar orbits, and orbits in three dimensions.

We provide further insights into the gravitational properties of this annulus and describe our computer algorithms and programs. We study a number of periodic orbits, giving them names to aid identification.

‘Ellipses extraordinaires’ which are bisected by the annulus, have no gravitating matter at either focus and represent a fundamental departure from the normal association of elliptical orbits with Keplerian motion. We describe how we came across this type of orbit and the analysis we performed. We present the simultaneous differential equations of motion of ‘ellipses extraordinaires’ and other orbits as a mathematical challenge. The ‘St.Louis Gateway Arch’ orbit contains two ‘instantaneous static points’ (ISP).

Polar elliptical orbits can wander considerably without tending to form other kinds of orbit. If this type of orbit is favoured then this gives a similarity to spiral galaxies containing polar orbiting material.

Annular oscillatory orbits and rotating polar elliptical orbits are computed in isometric projection. A ‘daisy’ orbit is computed in stereo-isometric projection.

The singularity at the centre of the SGA is discussed in relation to mechanics and computing, and it appears mathematically different from a black hole.

In the Appendix, we prove by a mathematical method that a thin plane self-gravitating Newtonian annulus, free from external influence, exhibiting radial gravitation that varies inversely with the radius in the annular plane, must have an area mass density which also varies inversely with the radius and this exact solution is the only exact solution.

### 3. Contents

p.1 .....	<b>1.</b> Preview picture.
p.2 .....	<b>2.</b> Abstract.
p.3 .....	<b>3.</b> Contents.
p.4 .....	<b>4.</b> Introduction.
p.4 .....	<b>5.</b> The full analytical equations for gravitation of the SGA.
p.6 .....	<b>6.</b> Orbital apogee ranges.
p.7 .....	<b>7.</b> Gravitational potential.
p.11 .....	<b>8.</b> Escape velocity - some practical considerations.
p.13 .....	<b>9.</b> The normalized equations of motion.
p.14 .....	<b>10.</b> Our algorithms, programs and equipment.
p.16 .....	<b>11.</b> Orbits in the annular plane (the $x,y$ plane).
p.17 .....	<b>12.</b> Isomorphism.
p.18 .....	<b>13.</b> Polar orbits ( <i>i.e.</i> in a plane perpendicular to the annulus, passing through its centre, such as the $x,z$ plane).
p.19 .....	<b>13.1</b> Chaotic orbit.
p.19 .....	<b>13.2</b> ‘St.Louis Gateway Arch’ orbits. Instantaneous static points.
p.19 .....	<b>13.3</b> ‘Ellipse extraordinaire’ orbits and a mathematical challenge.
p.26 .....	<b>13.4</b> ‘Crab’ orbits.
p.26 .....	<b>13.5</b> ‘Needle and thread’ orbit.
p.26 .....	<b>13.6</b> ‘Goldfish’ orbits.
p.26 .....	<b>13.7</b> ‘Alpha’ orbits.
p.26 .....	<b>13.8</b> ‘Propeller’ orbit.
p.26 .....	<b>13.9</b> ‘Centre target’ orbits with further analysis and discussion.
p.29 .....	<b>13.10</b> ‘Circular string-mat’ orbit.
p.29 .....	<b>14.</b> Non-planar orbits.
p.29 .....	<b>14.1</b> ‘Ball of string’ orbit.
p.31 .....	<b>14.2</b> Computing orbits in three dimensions.
p.31 .....	<b>14.3</b> ‘Daisy’ orbits.
p.32 .....	<b>14.4</b> Annular oscillatory orbits.
p.34 .....	<b>14.5</b> Rotating polar elliptical orbit.
p.36 .....	<b>15.</b> Brief further discussion.
p.37 .....	<b>16.</b> Appendix: Justification for the assumption of the area mass density varying inversely with the radius.
p.40 .....	<b>17.</b> References and Notes.
p.40 .....	<b>18.</b> Acknowledgements.

## 4. Introduction

We suspected, when computer modelling gravitating annuli, that it might be possible to arrive at the full analytical equations for gravitation in three dimensions, caused by a particular mathematical self-gravitating Newtonian thin plane annulus, having an area density inversely proportional to the radius, defined more precisely in the next section. (Note: In normal usage ‘annulus’, coming from the Latin meaning a ‘ring’, implies that an annulus contains a central hole, but here we use the term in a broader mathematical sense, including cases where the hole becomes vanishingly small.)

We found [1] for this annulus that it was possible to bypass the elliptic function problem which would normally be encountered when studying the off-axis properties of a physical system involving rings. Given additional features of this annulus that will later become apparent, we called this annulus the ‘special gravitating annulus’ or ‘SGA’. We discuss the role that a mechanically deceptive orbit, which we call the ‘ellipse extraordinaire’, played in bridging the gap from computing to mathematics, enabling us to obtain the gravitational field equations for this annulus, assisted by the Wolfram Integrator. Here we describe our computational results for the orbital properties of this annulus, and we provide further insights into its gravitational properties.

## 5. The full analytical equations for gravitation of the SGA

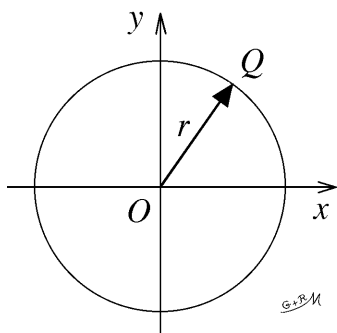


Figure 1: The annular plane is the  $x,y$  plane.

The SGA in Fig.1, with centre  $O$ , extends in the  $x,y$  plane to infinity. At the point  $Q$  on the annulus, at radius  $r$  from  $O$ , the area mass density  $\sigma$  is given by

$$\sigma = \frac{k}{r} \quad (r > 0) \quad (1)$$

where  $k$  is a constant, characterizing the annulus. Our mathematics [1], using Newton’s inverse square law, gives for the component of gravitation  $g_z$  parallel to the  $z$ -axis at a general point  $P$  in the  $x,z$  plane, see Fig.2,

$$g_z = \frac{2\pi Gk}{R} \quad (R > 0, z > 0) \quad (2)$$

acting towards the annular plane, where  $G$  is the gravitational constant. (Note:  $r$  in Fig.1 is in the  $x,y$  plane, and  $R$  in Fig.2 is in the  $x,z$  plane.) The function expressed by equation (2) is cylindrically symmetric around the  $z$ -axis, and on the annular plane itself,  $g_z$  is zero. Henceforth, regarding the annular plane (the  $x,y$  plane) as horizontal, then above this plane,  $g_z$  acts downwards, and below this plane  $g_z$  acts upwards, like a mirror reflection of the gravitation above. (Note: Orbital computations are not reflected, the particle passes through the annular plane, sometimes at quite glancing angles.)

In three dimensions, it follows from equation (2) and the symmetry discussed above, that the iso- $g_z$  surfaces are hemispheres, so they make semicircles where they intersect

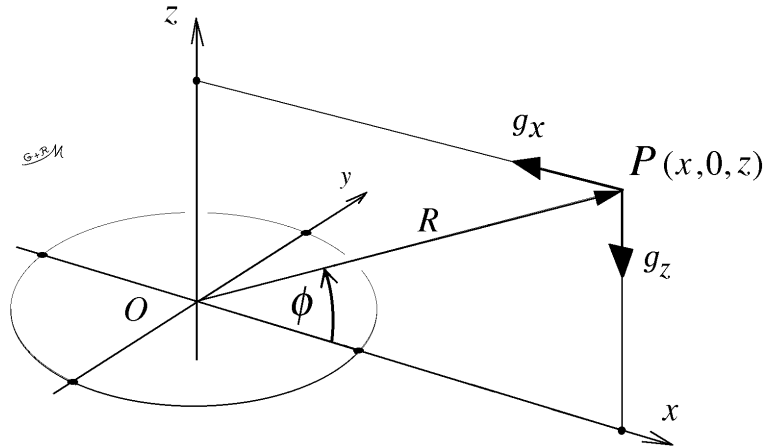


Figure 2: The three-dimensional geometry with the  $x$ -axis chosen to pass directly beneath the general point  $P$ , giving its co-ordinate position as  $(x, 0, z)$ , similar to our previous analysis [1]. (If the point  $P$  be located at  $(x, y, z)$ , then see Fig.16, page 31.)

any chosen polar plane such as the  $x, z$  plane in Fig.3, which shows just one quadrant. We first obtained our data by computer modelling of the SGA using a distribution of hundreds of thousands of mass points and summing the effect of each such point, later designing algorithms to plot iso-gravitational component contours, particularly to study  $g_x$ , but it came as a surprise to us to find that these iso- $g_z$  contours were very exactly circular. This provided us with some of the incentive to find a mathematical explanation. Our ‘candle-flame pattern’ of iso- $g_x$  contours, obtained in a computer run of many hours before we had arrived at equation (4) below, is given in reference [1], (although what appeared there was not our submitted data, but a graphically processed picture).

For now, notice that for any point  $P$  in Fig.2, equation (2) indicates that  $g_z$  is inversely proportional to the radius, not the radius squared, and on the  $z$ -axis itself

$$g_z = \frac{2\pi Gk}{z} \quad (z > 0), \quad (3)$$

( $z < 0$  is covered by regarding gravitation as being ‘reflected’ across the annular plane). The latter equation is the only gravitational equation that can easily be obtained using calculus applied to a point on the axis of the annulus, elsewhere, more complicated mathematics is required [1].

The component of gravity  $g_x$  parallel to the annular plane acting radially towards the  $z$ -axis (see Fig.2), we found [1] to be given by

$$g_x = \frac{2\pi Gk}{R} \left( \frac{1 - \sin \phi}{\cos \phi} \right) \quad (0 \leq \phi \leq \frac{\pi}{2}, R > 0). \quad (4)$$

The function is cylindrically symmetric around the  $z$ -axis and reflects across the annular plane. As  $\phi$  tends to  $\frac{\pi}{2}$ , the numerator tends to zero faster than the denominator, giving

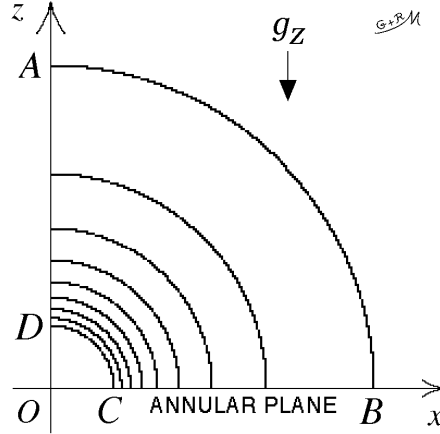


Figure 3: Iso- $g_z$  contours of the SGA. In Section 7, a particle of unit mass is taken around the cycles  $CDABC$  and  $OABO$ .

$g_x = 0$  on the  $z$ -axis, as expected. On the annular plane, where  $\phi = 0$  and  $R = x$ , then equation (4) gives

$$g_x = \frac{2\pi Gk}{x} \quad (x > 0). \quad (5)$$

( $x < 0$  is covered by the cylindrical symmetry, the gravitational component parallel to the annular plane, pointing radially inwards, is regarded as positive, so on the negative  $x$ -axis,  $g_x$  is positive, pointing towards  $O$ .) On the annular plane, the  $x$ -axis being equivalent to any other radial line through  $O$ , then equation (5) implies that the radial gravity  $g_r$  in the annular plane is given by

$$g_r = \frac{2\pi Gk}{r} = \frac{V_{rot}^2}{r} \quad (r > 0) \quad (6)$$

where  $V_{rot}$  is the speed of circular orbits (centred on  $O$ ) in this plane. Thus

$$V_{rot} = \sqrt{2\pi Gk} \quad (7)$$

and is independent of the radius.

## 6. Orbital apogee ranges

Comparing equations (3) and (5), it is seen that the way gravitation  $g_z$  on the  $z$ -axis varies, acting towards  $O$ , is identical to the way in which the gravitation  $g_x$  varies along the  $x$ -axis, also acting towards  $O$ . This means that if a particle be launched radially outwards with a constant velocity from the circumference of a small circle centred on  $O$ , as in Fig.4, then its range to apogee (point  $A$ ) when launched up the  $z$ -axis must equal its range to apogee (point  $B$ ) when launched along the  $x$ -axis: this provides one basic check of the accuracy of our orbit computations, the results being given in this diagram. (Faint range circles are plotted in case the  $x$  and  $z$  scales in the final Fig.4 are unequal.)

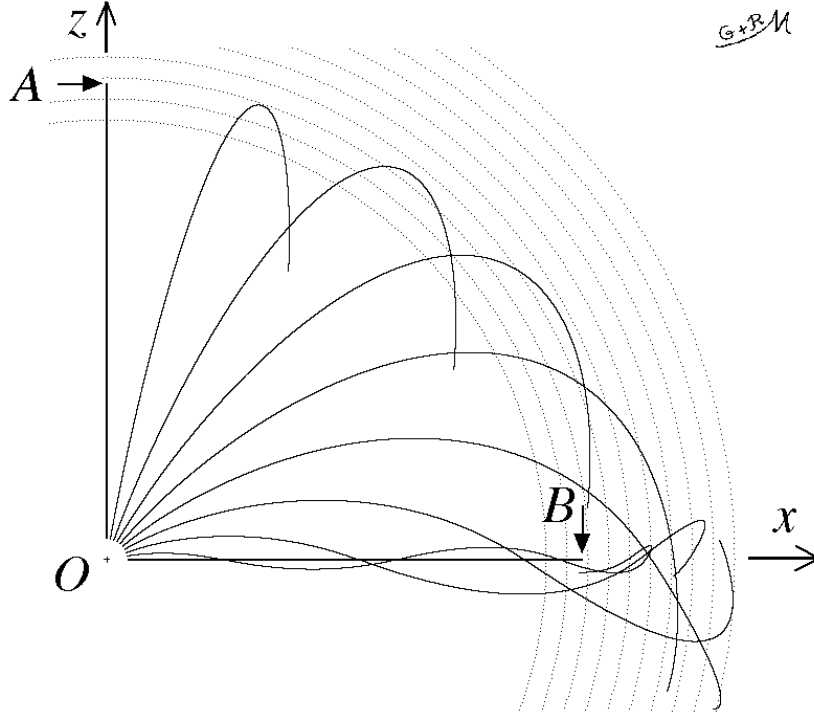


Figure 4: The ranges to which a particle reaches at apogee are seen for these orbits. The particle is launched with constant velocity radially from points spaced by  $10^\circ$  around a small launch circle centred on  $O$ . The range up the  $z$ -axis to point  $A$  is equal to the range along the  $x$ -axis to point  $B$ . (Note: a ‘pictorial pixelization problem’ may cause horizontal and vertical pieces of the much more accurately calculated orbits not to show, especially on printout. The one pixel widths of the axial orbits have been doubled here which may prevent them from vanishing.)

Other orbits given in Fig.4 correspond to  $10^\circ$  increments of launch angle around the small launch circle. When launched close to the annular plane, the particle has a greater range than when launched precisely along the  $x$ -axis, because the particle wanders above and below the annular plane into regions where  $g_x$  above and below the plane is slightly less, following the angular function given in equation (4). Also, explained shortly, the gravitational equipotential contours (in the polar plane) are not circular, but cut outwardly into the annulus at an inclination of  $45^\circ$ , so when a particle is pulled perpendicularly away from the annulus, its potential energy rises and this becomes available to project the particle to a greater range.

## 7. Gravitational potential

It may be thought that since the gravitational force varies identically along the  $z$  and  $x$  axes respectively, and they meet at  $O$ , then the gravitational potential at points

placed at equal distances from  $O$  on either axis, ought to be identical. However, this is not the case. This becomes apparent by analyzing the work  $W$  done in taking a particle once around the closed path,  $CDABC$  in Fig.3, (where  $CD$  and  $AB$  are quarter circular arcs) and since the field is conservative, the total cyclic work must be zero, given by

$$\oint_{CDABC} dW = \int_{CD} dW + \int_{DA} dW + \int_{AB} dW + \int_{BC} dW = 0 \quad (8)$$

or

$$W_{CDABC} = W_{CD} + W_{DA} + W_{AB} + W_{BC} = 0. \quad (9)$$

Two useful equations when dealing with such problems, which use equations (2) and (4), and the geometry of Fig.5, are the radial component of gravitation  $g_R$  given by

$$g_R = g_x \cos \phi + g_z \sin \phi = \frac{2\pi Gk}{R} \quad (0 \leq \phi \leq \frac{\pi}{2}, R > 0) \quad (10)$$

and  $g_\phi$  the circumferential or transverse component of gravity (directed towards the outer region of the annulus) given by

$$g_\phi = -g_x \sin \phi + g_z \cos \phi = \frac{2\pi Gk}{R} \left( \frac{1 - \sin \phi}{\cos \phi} \right) \quad (0 \leq \phi \leq \frac{\pi}{2}, R > 0), \quad (11)$$

thus  $g_\phi = g_x$  and  $g_R = g_z$ . (Note: The Cartesian and polar components, illustrated in Fig.5, must not be mixed in a mechanical analysis.) The work required to pull a unit mass quasi-statically around the arc  $C$  to  $D$ , *i.e.* away from the annular plane, is positive and, using equation (11), is given by

$$\begin{aligned} W_{CD} &= \int_0^{\frac{\pi}{2}} g_\phi R d\phi = \int_0^{\frac{\pi}{2}} \frac{2\pi Gk(1 - \sin \phi)}{R \cos \phi} R d\phi = 2\pi Gk \int_0^{\frac{\pi}{2}} (\sec \phi - \tan \phi) d\phi \\ &= 2\pi Gk \left[ \log_e (\sec \phi + \tan \phi) + \log_e \cos \phi \right]_0^{\frac{\pi}{2}} = 2\pi Gk \left[ \log_e (1 + \sin \phi) \right]_0^{\frac{\pi}{2}} \\ &= 2\pi Gk \log_e 2, \end{aligned} \quad (12)$$

where the radius  $R$  of the quadrant cancels within the expression. Hence it similarly follows that

$$W_{AB} = -2\pi Gk \log_e 2, \quad (13)$$

the negative sign indicating that work is done by the system against an external supporting force applied to the mass, when it is allowed to follow the arc  $A$  to  $B$  in quasi-static fashion. The work done in pulling the unit mass quasi-statically from  $D$  to  $A$  is, making use of equation (3), given by

$$W_{DA} = \int_{R_D}^{R_A} g_z dz = \int_{R_D}^{R_A} \frac{2\pi Gk}{z} dz = 2\pi Gk \log_e \left( \frac{R_A}{R_D} \right). \quad (14)$$

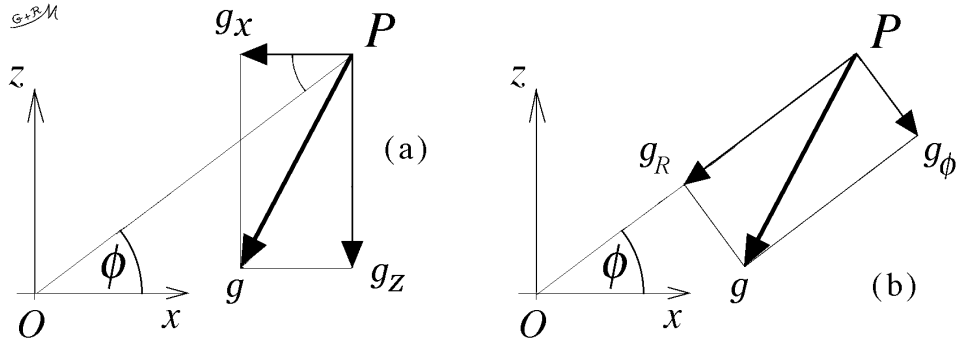


Figure 5: The gravitation  $g$  acting at  $P$  is resolved into (a) Cartesian or (b) polar components.

Similarly, using equation (5),

$$W_{BC} = - \int_{R_C}^{R_B} g_x dx = - \int_{R_C}^{R_B} \frac{2\pi Gk}{x} dx = -2\pi Gk \log_e \left( \frac{R_B}{R_C} \right) \quad (15)$$

where  $R_A$ ,  $R_B$ ,  $R_C$ , and  $R_D$ , are the radii of the respective points  $A$ ,  $B$ ,  $C$ , and  $D$  (in Fig.3). Since  $R_A = R_B$  and  $R_D = R_C$  then the radii ratios in (14) and (15) are identical, so  $W_{BC} = -W_{DA}$ . The summations given in equations (8) and (9) can now be done, whence the work done in taking a unit mass around the given cycle comes to zero, as it must.

A simple cycle apparently exists, however, where serious trouble is encountered. This consists in attempting to find the cyclic work in taking a particle of unit mass around the cycle  $OABO$  in Fig.3. Aside from the problem of taking the logarithms of infinite radii ratios—perhaps this effect cancels for the two straight parts of the cycle  $OA$  and  $BO$  along which the particle travels away from and towards  $O$  respectively—but this leaves the finite work in travelling around the arc  $A$  to  $B$ , a portion of the cycle where the particle does work on the external world. This suggests that it might be possible to devise a machine using the gravitational properties of this annulus to make a perpetual motion machine of the first kind, having no other effect than to continuously make work. Of course, this is impossible. The SGA obviously has educational potential in assisting those who study it, to respect infinities, for in the centre of this annulus, forces and gravitation tend to infinity. To resolve this problem, the cycle  $OABO$  should be considered as a limiting case of the original cycle  $CDABC$ , where the radius of the arc  $CD$  tends to zero. But the work required in travelling around this arc does not vanish, but remains at the constant value given by equation (12), thus preventing the construction of perpetual motion machines. However, the centre of this annulus certainly possesses some interesting properties, not only in causing serious difficulties concerning how to deal with the computation of orbits near to  $O$ , but also with basic issues in Newtonian mechanics, discussed later in section 13.9 ‘Centre target’ orbits.

It is now apparent that although gravitation varies identically along the  $x$  and  $z$  axes, and they meet at  $O$ , the gravitational potentials on these two axes are displaced from each other. A point on the  $z$ -axis at any given distance from  $O$ , has a gravitational potential higher by the constant quantity,  $2\pi Gk \log_e 2$ , compared to the potential at a point at the same distance from  $O$  on the  $x$ -axis. This leads to another problem concerning what happens at large radii from  $O$ . It is customary to regard the potential of gravitation at an infinite distance from a gravitating system as zero. When working out an escape velocity, for example, this is the velocity that would give a particle just enough energy so that, when it reaches infinity, the velocity would be zero. The gravitational potential at a point is normally reckoned downwards from the zero value at an infinite distance away, and is the negative of the energy required to effect the escape of a unit mass. But in the case of the SGA, the  $z$ -axis and the  $x$ -axis have a step in potential between them, yet when extrapolated to infinity they both ought to end up at the same zero potential. How is this to be resolved?

This particular problem—which influences computer algorithms concerning how to calculate gravitational potential—vanishes underneath another problem caused by encountering infinities yet again. It will be seen from equation (10), that the radial component of gravitation  $g_R$  is inversely proportional to the radius, on any fixed radius vector in any direction from  $O$ . To avoid the complication of integrating along curved orbits, it may be imagined that a frictionless radial guiding rail is constructed from  $O$ , at any chosen angle to the annulus. A particle of unit mass, starting from radius  $R$ , is projected along this rail to infinity, with a view to calculating the escape velocity, and hence the kinetic energy required. The latter is the same as the work  $W$  required to pull the particle from the given point at radius  $R$ , to infinity and, using equation (10), this gives

$$W = \int_R^\infty g_R dR = \int_R^\infty \frac{2\pi Gk}{R} dR = 2\pi Gk \left[ \log_e R \right]_R^\infty = \infty. \quad (16)$$

The infinite result of equation (16) implies:-

(a) It is not possible to compute equipotential contours for an SGA relative to the zero potential assumed to exist at an infinite radius, however, they can be plotted as the loci of points that trace lines perpendicular to the gravitational field lines, as in Fig.6(a) where the gradient of a gravitational field line is obtained from equations (2) and (4) as the ratio  $g_z/g_x$  at any particular point. By moving perpendicularly to this direction a very small distance and repeating the procedure, we are able to construct a computer algorithm to plot the equipotential contours, shown.

The map of data in Fig.6(a) is valid for  $z > 0$ , but is not valid for the potential exactly on the mathematically thin annular plane. The contours in this map are computed down to just above the  $x$ -axis, where a mathematical discontinuity exists and the gravitational field lines suddenly change direction, becoming parallel with the annular plane. Of course, we can give this annulus a finite thickness and a vertical distribution of matter, and study such systems in more detail. This requires constructing an annulus made of a distribution of point masses, then using Newton's inverse square law and visiting every point in the model, the gravitational contributions for all the points are summed, to

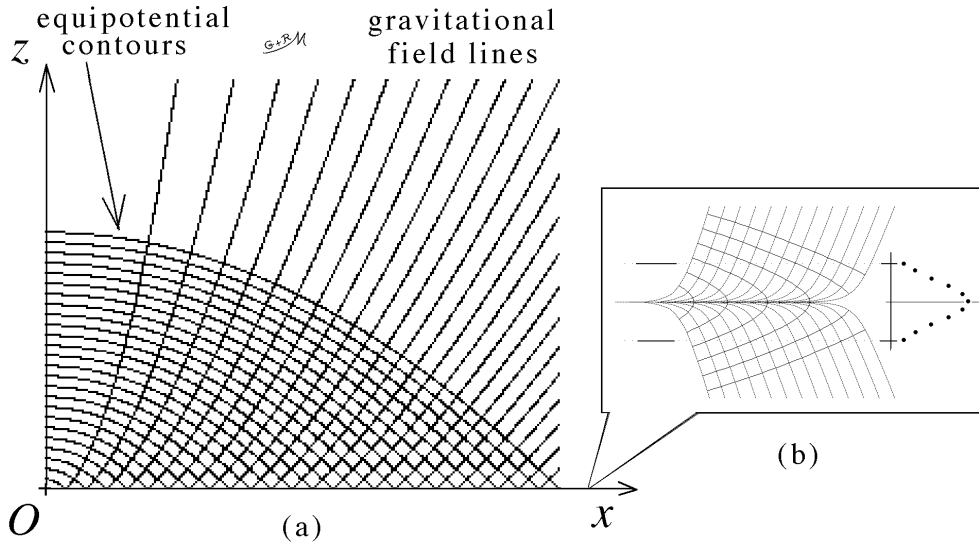


Figure 6: (a) A map of gravitational field lines and orthogonal equipotential contours in one quadrant, but it does not give data on the  $x$ -axis itself. (b) An indication of what happens inside a thin layer of finite thickness. This thin layer is itself composed of eleven thin layers with a vertical mass distribution given by the small black dots in the very small graph on the right.

give the gravitational components at each of the many points of interest required to plot various curves. This procedure is done in Fig.6(b) for a thickness distribution of matter that follows the same curve as the velocity component distribution of gas molecules in Maxwell-Boltzmann statistics (indicated just to the right of the contour map), but we refrain from pursuing this in depth in the present paper.

(b) Sometimes it is useful to compare with gravitational situations, equivalent situations in electrostatics, such as the ‘infinitely deep potential well’ exhibited by a finite point charge. Equations such as (10) suggest that a similarly deep gravitational well occurs at the centre of an SGA, meaning that provided we keep away from the centre, then we will ourselves not become gravitationally dragged into this infinitely deep potential well. However, wherever we happen to be located with respect to an SGA, if we launch a particle towards infinity with a finite velocity, the particle never gets there (this follows from equation (16)), so the presence of an SGA already places a hypothetical general observer infinitely far down a gravitational well, even when the observer is not located at the centre [2]. This topic is discussed further in section 13.9 ‘Centre target’ orbits.

## 8. Escape velocity - some practical considerations

Despite these mathematical peculiarities, it is still possible to be practical, for example, instead of attempting to calculate the escape velocity to infinity, let us calculate the velocity  $v$  that will take a particle of mass  $m$ , launched radially from a point at distance

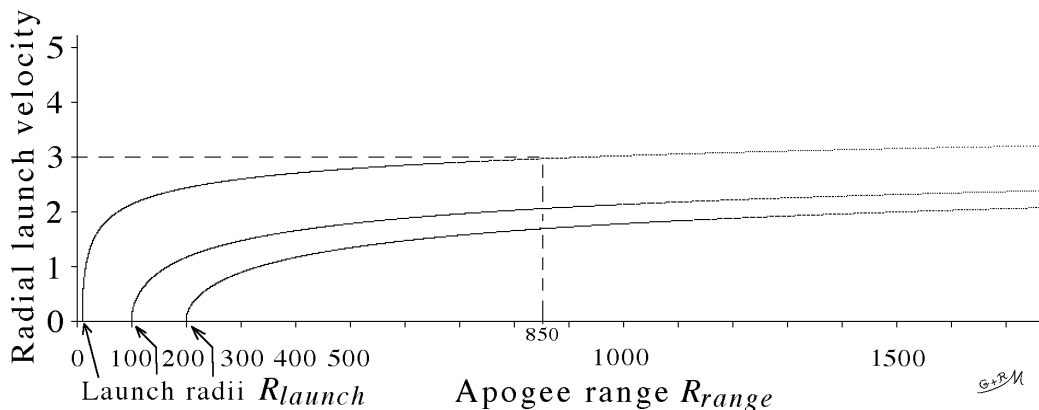


Figure 7: A particle launched from a radius  $R_{launch}$  along a frictionless radial guiding rail, or along the  $z$  or  $x$  axes respectively, travels to an apogee range  $R_{range}$  given by equation (18). The three curves given are for  $R_{launch}=10$ , 100, and 200 respectively.

$R_{launch}$  along the  $x$  or  $z$ -axis from  $O$ , or along a frictionless radial guiding rail, to an apogee range  $R_{range}$ . This launch velocity and apogee range are related by

$$\frac{1}{2}mv^2 = 2\pi Gkm \log_e \frac{R_{range}}{R_{launch}} \quad (17)$$

using the same procedure that yielded equation (16), whence

$$R_{range} = R_{launch} \exp\left(\frac{v^2}{4\pi Gk}\right). \quad (18)$$

This equation is plotted in Fig.7 for three launch radii. As an example, the curve for innermost launch ( $R_{launch} = 10$ ) gives the result that a radial launch velocity of 3 units (these are ‘normalized units’ discussed next in Section 9) gives an apogee range of 850 units (these are ‘screen units’ with a one to one correspondence with the units of distance in our computer programs, we give details of any different scales that we use where appropriate). The curves demonstrate that as the launch velocity is increased towards a threshold, the range to apogee enormously increases. It might be said, to all intents and purposes, that a particle launched with sufficient finite speed travels so enormously far, that this is as good as reaching infinity, but of course, mathematics says otherwise, the equations yield an infinite escape velocity. Whilst the graphs in Fig.7 suggest that asymptotes might be practically constructed, the mathematics indicates that no such asymptotes exist, all horizontal lines constructed in Fig.7 when projected, eventually cut a given mathematical curve. Curves corresponding to launching a particle from closer to  $O$ , require larger and larger launch velocities to cause the particle to travel significant distances to apogee. (The best way to become familiar with these curves is to experiment with their computer plotting.)

A practical consequence of equation (18) is that it is very noticeable how an orbital plot which is fully contained on the computer screen, can run very far off-screen with a slight increase in orbital launch speed. (While wondering what to do, you may be lucky enough, several minutes later, to see the particle on its travels, temporarily back on-screen!)

## 9. The normalized equations of motion

It is convenient to normalize the equations by setting  $V_{rot}$  in equation (7) equal to unity, so then

$$2\pi Gk = 1. \quad (19)$$

All velocities can now be expressed in terms of multiples of unity, unity being the circular orbit speed for all such orbits in the plane of the SGA, the units of velocity in Fig.7 are expressed in this manner. Following normalization, equations (2) and (4) then become

$$g_z = \frac{1}{R} \quad (20)$$

and

$$g_x = \frac{1}{R} \left( \frac{1 - \sin \phi}{\cos \phi} \right) \quad (21)$$

respectively, valid for  $0 \leq \phi \leq \frac{\pi}{2}$ , and  $R > 0$ . The functions are cylindrically symmetric around the  $z$ -axis and reflect across the annular plane as discussed earlier (Section 5).

We have used the sign convention that gravitation on the surface of the Earth is positive but acts downwards. Hence, in computer programs and equations using Cartesian coordinates, the respective acceleration components,  $a_x$  and  $a_z$ , are obtained in the first quadrant of the  $x, z$  plane by setting  $a_x = -g_x$  and  $a_z = -g_z$ , with appropriate changes of sign, where needed, in the other quadrants (the arrows in the corners of Fig.11(a) later are of assistance here). Hence, using the normalization expressed by equation (19), and using  $x = R \cos \phi$  and  $z = R \sin \phi$ , then equations (20) and (21) yield in Cartesian form,

$$a_z = \frac{d^2z}{dt^2} = -\frac{1}{R} = -\frac{1}{\sqrt{x^2 + z^2}} \quad (22)$$

valid for all  $x$ , with  $z > 0$ , and

$$a_x = \frac{d^2x}{dt^2} = -\frac{1}{x} \left( 1 - \frac{z}{\sqrt{x^2 + z^2}} \right) \quad (23)$$

also valid for all  $x$ , with  $z > 0$ , (note: as  $x \rightarrow 0$  this expression  $\rightarrow 0$  not  $\infty$ ). The reversal of the  $x$  and  $z$  components of acceleration for a particle crossing the  $z$  and  $x$  axes respectively, has its similarities to the switch to the opposite direction of the acceleration of a mass on a spring as it passes through its midpoint of oscillation.

A pair of simultaneous differential equations of motion for a particle orbiting in the  $x, z$  plane, valid for  $z > 0$ , can be obtained from equations (22) and (23) as follows:

$$x \frac{d^2x}{dt^2} + z \frac{d^2z}{dt^2} = -1 = \frac{d^2z}{dt^2} \sqrt{x^2 + z^2} \quad (24)$$

but this is not necessarily the most convenient form in which to try to obtain solutions for the equations of polar orbits, although it is interesting to compute and plot the various parts of this simultaneous equation pair to see how they behave during computer runs.

## 10. Our algorithms, programs and equipment

There is scarcely a need to compute circular orbits in the annular plane (the  $x,y$  plane), apart from the overriding reason that these orbits are a gold-standard for checking the accuracy of orbit algorithms. For example, when non-circular orbits are obtained with unknown equations, especially in the  $x,z$  plane, the question arises as to whether these shapes relate to genuine gravitational and orbital properties of the annulus, or are influenced by computational inaccuracies. Three ways to check this are:

1. Determine if the computer program can yield accurately circular orbits (in the  $x,y$  plane) under the influence of gravitational fields as intense as those which occur around the orbital paths of the non-circular orbits (not necessarily in the  $x,y$  plane), particularly at closest approach to  $O$ .

2. If periodic orbits change size then the computer program is not obeying the conservation of energy. Likewise it may become apparent that chaotic orbits may be growing gradually larger. The remedy is to increase the computational accuracy by reducing  $Dt$ , discussed below, and to increase the number of computational steps. (In developing our computer programs we found a method of getting very close compliance with the conservation of energy using a program that runs ten times faster, but given that we have not completed our investigations of this method, we have not used it in the orbital computations of the present paper. We hope to discuss it on another occasion.)

3. In the case of a chaotic orbit, it is always necessary to test the effect of a reduction of the time interval  $Dt$ , to see if the computed orbit remains the same shape, and find an optimum value that gives the required accuracy over the chosen length of the computed orbit, in a reasonable computing time.

### Our algorithm followed this sequence:

**Stage 1.** Choose a numerical value for the short time interval  $Dt$ , familiar as  $\delta t$  in differential calculus. In mathematics, this interval tends to zero, but in computing this can only be approximated. In our computer programs we call this time interval ‘Dt’, (this parameter and various others are not italicized within the programs we give here).

**Stage 2.** Specify the initial particle position  $x,y,z$  and the respective launch velocity components,  $v_x,v_y,v_z$ .

**Stage 3.** Plot the particle position at  $x,y,z$ . In the case of three dimensions this can be done with plan and elevation views, or isometric projection, such as in the ‘Preview picture’ and in Figs.17, 18 and 19 (pages 32-34). Fig.17 includes a stereo-isometric pair.

**Stage 4. Either 4(a)** visit every mass point in a gravitating annular model, typically 100,000 such points, and sum the contributions to the gravitational

components at  $x,y,z$ , the current position of the orbiting particle. This involves considerable computing time.

**Or 4(b)** calculate the gravitational components at point  $x,y,z$ , if the analytical equations are available—they now are for the SGA [1], and we do this here, using equations (20) and (21), having regard to the various conditions imposed by the symmetry discussed in Section 5. Geometric details for computing orbits in three dimensions are given in Section 14.2 (page 31).

**Stage 5.** Obtain the respective acceleration components,  $a_x$ ,  $a_y$  and  $a_z$ , by placing each component equal to the corresponding gravitational component, respectively, with or without a change of sign according to the quadrants of the Cartesian set of orthogonal planes through  $O$  corresponding to the position of the particle. (There are neat ways of doing this within a program.)

**Stage 6.** In the time interval  $Dt$ , update the values of  $x$ ,  $y$ , and  $z$  respectively, as follows (where ‘ $\leftarrow$ ’ means ‘update the value of the variable on the left with the computed expression on the right’ as in LINE 140 Program 1 on page 16.)

$$\begin{aligned}x &\leftarrow x + v_x \cdot Dt + 0.5 a_x \cdot Dt^2, \\y &\leftarrow y + v_y \cdot Dt + 0.5 a_y \cdot Dt^2, \\z &\leftarrow z + v_z \cdot Dt + 0.5 a_z \cdot Dt^2,\end{aligned}$$

where  $v_x$ ,  $v_y$  and  $v_z$  are the velocity components parallel to the  $x$ ,  $y$  and  $z$  axes respectively.

**Stage 7.** Similarly the new values of  $v_x$ ,  $v_y$  and  $v_z$ , are obtained as follows

$$\begin{aligned}v_x &\leftarrow v_x + a_x \cdot Dt, \\v_y &\leftarrow v_y + a_y \cdot Dt, \\v_z &\leftarrow v_z + a_z \cdot Dt.\end{aligned}$$

**Stage 8.** Cycle back to Stage 3, and repeat until a specified number of computations have been completed.

An example of our programs in BBC Basic (easily translated to certain other languages) is Program 1 (on page 16) for computing orbits in the  $x,y$  plane, generating Fig.8, discussed in the next section.

To run our programs, a BBC emulator suitable for use on a PC can be obtained by entering “bbc basic for windows” into the Google search facility. Our emulator was supplied by Human-Computer Interface Ltd. of Cambridge in the 1990s; we later found that this emulator worked very satisfactorily on a Power Macintosh G3. By modern standards this computing system, which we still use, is slow, but it has several benefits. For example, when doing a computation lasting several hours, during which we wonder what will happen, this can be an exciting time for productive thinking, especially when watching orbits forming. However, by the 1990s, we had considerable experience of mainframe computing but we go back further into the 1960s when it was necessary to purpose-build computers, particularly in relation to our other researches, assisted by an equipment gift from IBM (provided that it was not used to go into competition with them!) and a Leverhulme Research Award. This experimental machine, built in the Medical School of Guy’s Hospital, was related to research into tessellations, an area

in which we still work. Later we used mainframe computers, developing FORTRAN IV and 77 programs to generate three-dimensional Voronoi tessellations, for example, and to control a machine we designed for use in industry. What we describe here relates to our activities at home, and we try to get the most out of our equipment. Another important aspect is having full control over our computing and we like the flexibility of penetrating problems by computing in the ways in which we wish, writing our own complete programs in FORTRAN or BBC Basic—this article contains plenty of examples of the results of this aspect of our work. We believe that much is to be gained in understanding the physical nature of problems by starting with the simplest programs to model them, and extending the programs in stages, following the requirements of the imagination. Some of our programs, of only twenty lines or so, can yield a wealth of data.

**Program 1 : Orbits in the annular plane ( $x,y$  plane).**

```

10 CLS : REM clears the screen. (A MODE number might be required
    depending upon the emulator type, such as in Program 2, page 18).
20 Dt=0.05
30 PRINT " Dt=" ; Dt ;
40 VDU29,1000;700 ; REM centres the picture (depends upon the
    emulator).
50 MOVE -5,0 : DRAW 5,0 : MOVE 0,-5 : DRAW 0,5 : REM origin marker.
60 x=0 : y=50 : vx=1.94 : vy=0 : REM the launch parameters.
70 PRINT " x=" ; x ; " y=" ; y ; " vx=" ; vx ; " vy=" ; vy
80 count%=0 : REM an integer variable
90 REPEAT
100 PLOT 69, x, y
110 r=SQR((x*x)+(y*y))
120 ar= -1/r : REM radial acceleration.
130 ax=ar*x/r : ay=ar*y/r : REM radial acceleration components.
140 x=x+vx*Dt+0.5*ax*Dt^2 : y=y+vy*Dt+0.5*ay*Dt^2
150 vx=vx+ax*Dt : vy=vy+ay*Dt
160 count%=count%+1
170 UNTIL count%=200000
180 END

```

**11. Orbits in the annular plane (the  $x,y$  plane)**

Circular orbits with unit speed obey the normalized version of equation (7) discussed in Section 9, but generally, depending on the launch velocity, the orbits are non-circular and take the form of rotating polar cycloids. By fine tuning the launch velocity, in LINE 60, of Program 1 above, it is possible to make an orbit closely retrace itself, such as the trefoil shapes of Fig.8(a), where the particle is launched parallel to the  $x$ -axis, from three positions on the  $y$ -axis, with  $v_x = 0.312$ , whence isomorphism becomes apparent, discussed below. Each trefoil pattern crosses the  $y$ -axis perpendicularly, so there are two

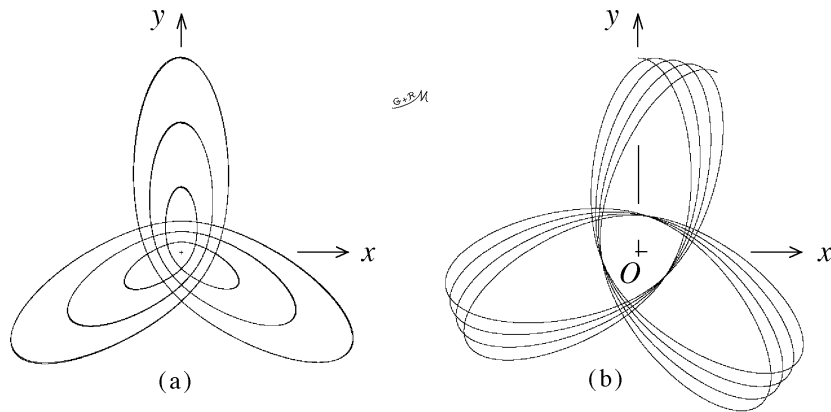


Figure 8: (a) A family of three isomorphic trefoil orbits. (b) Precession of a similar single orbit.

perpendicular launch velocities, the larger one corresponding to the inner intersection requires  $v_x = 1.94$ . (Of course, launching the particle with  $v_x = 1$  gives a circular orbit.)

Sooner or later, however, with sufficient cycles, retracing accuracy becomes lost, as in Fig.8(b), obtained with a launch speed  $v_x = 0.35$  chosen to illustrate precession. (However, we found that with the polar orbit called ‘ellipse extraordinaire’, described later, this orbit retraced itself accurately even throughout hundreds of cycles.) There are questions concerning the stability of orbital computations, sometimes numerical errors oscillate about the ‘true value’, but here we simply reduce  $Dt$  (like in LINE 20 of Program 1) until the accuracy desired is obtained.

## 12. Isomorphism

A fundamental property of all the orbits exhibited by a particle under the influence of the SGA is isomorphism. This is the characteristic, apparent in Fig.8(a), that when a particle is launched with a particular velocity vector, the same shaped orbit is produced regardless of the distance along a fixed radius vector from which the particle is launched. The speed of the particle varies around the orbital path, so at first it can be astonishing to see the same shaped orbit appearing rapidly for the innermost orbit, and slowly for the outermost orbit in a magnified form. An orbit of twice the size takes double the time to compute in twice the number of computing steps, determined by the value of  $Dt$  common to both orbits.

Isomorphism arises from the characteristic of the SGA that gravitation varies inversely with the radius. Consider, for example, two orbits, one of them a scaled-up version of the other, enlarged by a factor  $\beta$ . To every point on the inner orbit, is a corresponding point on the outer orbit, where the gravitational components are  $\beta$  times less. A particle on each orbit moving with the same speed  $v$  at both points, requires a force to act towards the radius of curvature of each orbit, this force being less in proportion to

the reciprocal of the radius of curvature. Such a force is exactly provided by the SGA, with gravity varying inversely with the radius.

Isomorphism can facilitate computing. If you wish to magnify an orbit, then keep the launch speed and direction the same, but launch the particle from a position further out in order to see a larger orbit, or further in to see a smaller one. The effect operates for all orbits, including in three dimensions. For orbits that go near to the centre of the SGA, where the gravitational fields are high,  $Dt$  should be reduced to maintain accuracy. This raises interesting mechanical, physical and computational questions, particularly in relation to ‘centre target’ orbits, discussed later in Section 13.9.

Circular orbits of constant speed in the annular plane are the simplest set of isomorphic orbits for this annulus.

### 13. Polar orbits

A rich variety of orbits is exhibited by a particle in a plane perpendicular to the annulus through  $O$ , like the examples seen in Fig.9 on page 20, or in Fig.13 on page 27, obtained with appropriate parameters inserted into a program, such as in LINES 20, 50 and 60 of Program 2 below (giving a different choice of method of centering the picture).

#### Program 2: Orbits in a polar plane, such as the $x,z$ plane.

```

10 MODE 8 : CLS : REM the mode number depends upon the emulator.
20 Dt=0.05
30 mx=800 : mz=500 : REM in this program example, choose these numbers
   to centre the picture.
40 MOVE mx-5,mz : DRAW mx+5,mz : MOVE mx,mz-5 : DRAW mx,mz+5
   : REM origin marker.
50 FOR X=50 TO 500 STEP 50
60 x=X : z=0 : vz=5/3 : vx=0 : REM launch parameters for ten ‘ellipses
   extraordinaires’.
70 count%=0
80 REPEAT
90 PLOT 69, mx+x, mz+z
100 r=SQR((x*x)+(z*z)) : az= -1/r : REM see equation (22).
110 IF z<0 THEN az=-az
120 IF z=0 THEN az=0
130 IF x=0 THEN 140 ELSE 150
140 ax=0 : GOTO 160
150 ax= -(1/x)*(1-ABSz/r) : REM see equation (23).
160 x=x+vx*Dt+0.5*ax*Dt^2 : z=z+vz*Dt+0.5*az*Dt^2
170 vx=vx+ax*Dt : vz=vz+az*Dt
180 count%=count%+1
190 UNTIL count%=10000*X/50
200 NEXT X
210 END

```

Given the cylindrical symmetry, all polar planes through the  $z$ -axis are equivalent, so here we choose the  $x,z$  plane as representative of all such planes. These orbits are discussed in more detail, as follows, (but two families, ‘ellipses extraordinaires’ and ‘centre target’ orbits, merit more detailed discussion and analysis). Referring to Fig.9, on page 20, the following orbits can be identified.

**13.1 Chaotic orbit** (Fig.9): An arbitrary choice of launch parameters for a particle yields, in general, a chaotic orbit. However, it became apparent to us, by adjusting the launch parameters, that various periodic orbits are possible.

**13.2 ‘St.Louis Gateway Arch’ orbits** (Fig.9): launched perpendicularly with  $v_x = 1.366$  from points on the  $z$ -axis. We gave this name to this orbit because the Gateway Arch in St.Louis represents the starting point of explorers travelling West [3], and perhaps we ourselves were embarking into unexplored territory here. This orbit contains two ‘instantaneous static points’ (ISP) where, for a brief instant, the speed of the particle is zero, so for an infinitesimal time interval, the particle scarcely moves. Since the kinetic energy has fallen to zero at such points, the work done against the potential of the gravitational field is at its greatest, so an ISP, if it occurs, does so at the furthest distance of the particle from  $O$ . However, the range to an ISP tends to be greater when it occurs near to the annular plane compared to when it occurs near to the  $z$ -axis, as in the ‘needle and thread’ and ‘alpha’ orbits which appear in Fig.13 later (on page 27). In the ‘Preview picture’, the close approximation to a ‘St.Louis Gateway Arch’ orbit assists with the three-dimensional display, as this orbit intentionally wanders in the  $x = y$  plane.

**13.3 ‘Ellipse extraordinaire’ orbits** (Fig.9) **with further analysis and a mathematical challenge**: Rather than present these orbits here as a *fait accompli*, we give some of the story concerning how they were found and why we investigated them further. Using the algorithm under Stage 4(a), described in Section 10 (page 14), we launched a particle perpendicularly from the  $z$ -axis, and watched it curving towards the annular plane, taking twenty minutes or so to reach it, such was the speed of our computations at that time [4]. We realized that by adjusting the launch speed, we might cause the particle to pass through the annular plane perpendicularly. After several days of parameter tuning, and using various methods to improve computing accuracy, we were greeted by an isomorphic family of astonishingly elliptical orbits. These orbits contain no gravitating matter at either of their foci, and are made mechanically possible, courtesy of the sheet of gravitating annular matter which bisects them.

We found the semi-minor to semi-major axis ratio of ‘ellipses extraordinaires’ close to 0.6 giving an eccentricity close to 0.8 and the particle passes through the annular plane with a speed of approximately 1.66. Earlier it seemed that ‘ellipses extraordinaires’ might have numbers associated with the ‘golden ratio’ (0.618... and 1.618...). This provided further motivation for us to obtain analytical equations for the gravitation of the SGA so as to improve the accuracy and speed of our computations and study this in more detail.

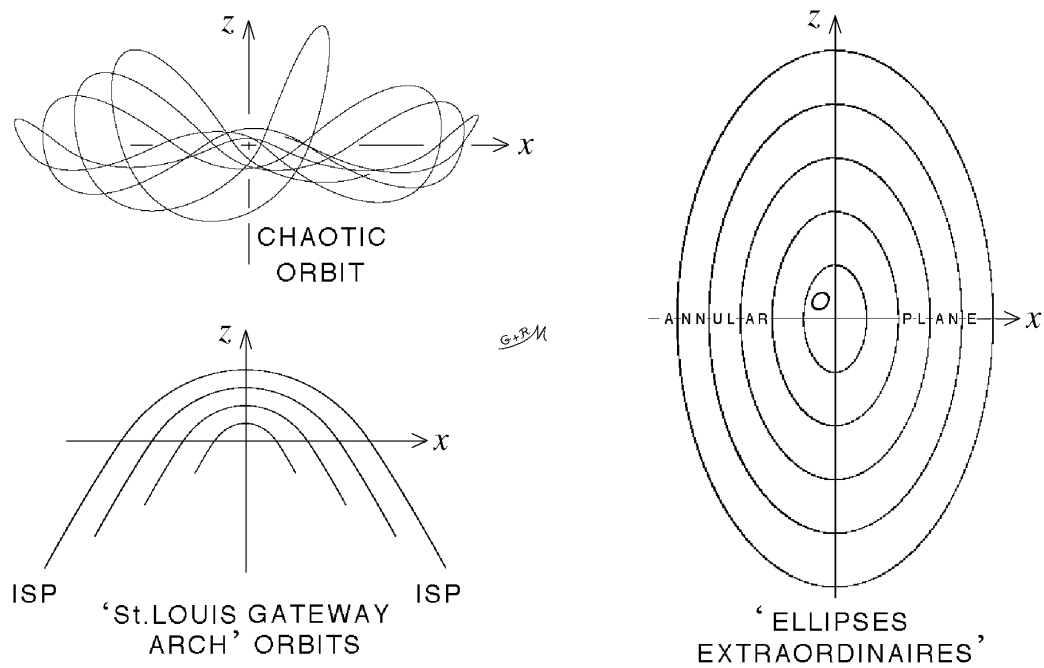


Figure 9: Three examples of polar orbits. The chaotic orbit is a single orbit, the other orbits are isomorphic families. In the case of a ‘St.Louis Gateway Arch’ orbit, the particle oscillates along the same track connecting the ‘instantaneous static point’ (ISP) at each end. Further polar orbital examples are given in Fig.13, page 27.

Initially we thought that the SGA was causing these elliptical orbits to form by behaving as if the annulus were mechanically equivalent to a mass concentrated at the focus of each particular elliptical orbit on the opposite side of the SGA. Whence, as the particle passes through the annular plane, this equivalent point mass would switch sides, allowing the other half of the elliptical orbit to be formed. We were attempting to deduce the full equations for the gravitation of the SGA and it appeared that these elliptical orbits could provide the necessary mathematical clues. Examining our programs and notes for April 2007, the situation then was that we knew how  $g_z$  varied according to equation (2), but we had not established its mathematical basis. We were struggling to understand the whole problem and this involved finding an equation for  $g_x$  in the polar plane.

By then we had developed a mathematical series method (see the Appendix) of overcoming the elliptic function problem, avoiding calculus, but we could not find a way to extend this method into three dimensions. (We developed this method to explain what our computer modelling was suggesting at that time: that there might be a ‘purely mathematical annulus’ giving a radial gravitation varying inversely with the radius.) Moreover the method did not tell us why the strength of gravitation at any point on the  $x$ -axis was equal to the gravitation at a point at the same distance from  $O$  on the  $z$ -axis which we knew to be true from our computing. Here is a diary entry (with some symbol formatting) illustrating how the elliptical orbits which we were then getting, suggested how we might ‘crack the mathematics’.

14 April 2007: ...computer running most of the day... we are getting hints of the ability to put a general formula to  $g_x(z, x)$ , we already have  $g_z(z, x)$ . The fact that we get elliptical orbits for a ratio of minor to major axes of 60%, or close to that, means that around this (particular) elliptical orbit, the combination of  $g_x$  and  $g_z$  must sum to produce the same field as the inverse square  $g$  law around the orbit. That gives a means of working out how  $g_x$  must vary.

It took us six more weeks to get the solution and to realize, *en route*, that this idea was not correct. To assist in the determination of the accuracy of the elliptical orbits and to find how closely the lines of action of orbital forces passed through the opposite focus, for a few weeks we used an ‘intermediate method’ to speed up our computing. We computed  $g_x$  in one-tenth degree steps around the circumference of one quadrant in the  $x, z$  plane, storing the results as a data file. By then we knew that an inverse radius law of gravitation applies to the SGA in three dimensions, so if  $g_x$  be known at any point on any radius vector, then it can immediately be computed for any other point on that radius vector. So then algorithm Stage 4(a) described in Section 10 (page 14), only needs performing once around a quadrant of constant radius and the data can then be used (with ‘fine scale’ interpolation) for subsequent orbit computations at much greater speed. We attempted to guess the mathematical angular function describing this data, given in Fig.10, but despite its simplicity, see equation (4), we did not succeed. This had to await our derivation of the equation itself.

Fig.10 shows some of our intermediate data, computed for five quadrants of radii 100 (this radius gives the strongest gravitational components in this diagram), 200, 300, 400 and 500 units, respectively. Examining the data for  $R = 100$ ,  $g_z$  computed around the quadrant starting from the  $z$ -axis, is seen to remain constant, suddenly dropping to zero as  $\phi \rightarrow 0$ . (How suddenly it falls gives a measure of modelling accuracy, the more accurate, the slower the program runs). But the value of  $g_x$  starting at  $\phi = 0$  (on the  $x$ -axis) has the same height as the ' $g_z$  plateau', decreasing to zero along the curve labelled the 'unknown function' as  $\phi \rightarrow 90^\circ$ . All such curves for quadrants of different radii are identical when multiplied by the appropriate vertical scaling factors, so only one needs to be computed.

Decades ago, when faced with tricky integrations, weeks could be spent attempting to do such integrations by hand. If this failed, this was followed by a journey to London and a search of the biggest mathematical manuals available in the Patents Office Library, just off Chancery Lane. But today the Wolfram Integrator is readily available on-line (involving us in a much shorter journey, a bicycle trip to the local Public Library to access the Internet). For us, this is a most wonderful animal, and like a trip to the zoo to see your first elephant, one wonders what kind of food you will be allowed to feed it. We fed the Wolfram Integrator with various expressions and received in return, huge expressions sometimes containing dozens of nested brackets, hypergeometric functions and imaginary numbers. Then suddenly the Wolfram Integrator gave us the answers we needed, and with a little translation, these answers enabled us to arrive at equation (4), with no elliptic functions appearing. So at last we knew that this 'mathematical voyage' is possible and this makes a great deal of difference to those inclined to do such things by hand and only our manual solution found its way into print [1] with none of this background story.

Our arrival at the equations (2) and (4) allowed us to pursue Stage 4(b) of our computer algorithm (see page 15). Fig.11(a) on page 24, gives the result of approximately three circuits of each 'ellipse extraordinaire', computed in 200,000 steps, making clear in which directions the gravitational components are pointing. These orbits took us seconds rather than many minutes to plot. With the far greater speed and accuracy we then

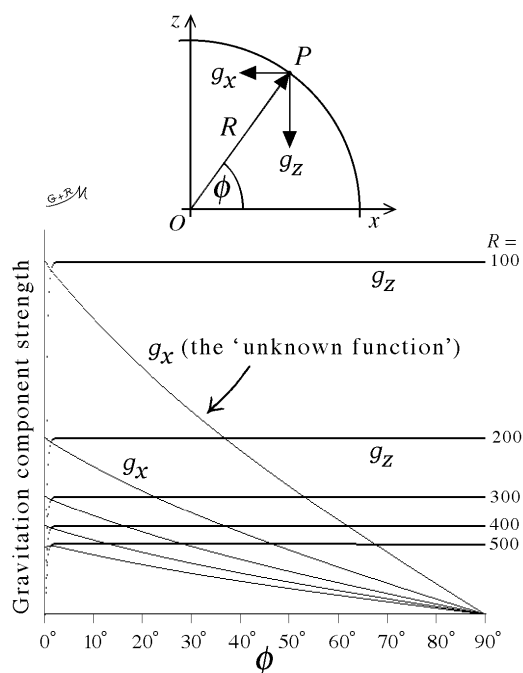


Figure 10: As point  $P$  travels around a quadrant of constant radius  $R$ ,  $g_x$  and  $g_z$  are computed and plotted.

found perhaps some significance in one of the launch numbers. ‘Ellipses extraordinaires’ are produced by launching a particle with velocity  $v_z = 1.66689 \pm 0.00002$  and  $v_x = 0$ , from points (except for  $O$ ) on the  $x$ -axis. This launch velocity appears to be very close to the simple mathematical ratio  $5/3$ , but our more recent computing makes us certain that it is very slightly greater than  $5/3$ , but until the simultaneous differential equations of motion (24) are solved, then we do not know what the significance of this is. To achieve this degree of accuracy  $Dt$  is considerably reduced and just the pieces of the elliptical orbits where they intersect the Cartesian axes are magnified and plotted on-screen, for a few cycles per orbit. The various images that are obtained allow us to ‘home in’ on the picture that very exactly repeats, thus to provide the most accurate figures we can obtain, as above, checked by further reductions of  $Dt$  down to 0.0001, using a linear image magnification of 1000, launching the particle from  $x=150$  units.

It then became clear, with the gravitational field equations then available, that ‘ellipses extraordinaires’ are not Keplerian. The vector force acting on the orbiting particle, see Fig.11(b), systematically wanders from pointing at the ellipse focus on the opposite side of the annulus. The direction  $\xi$  of the resultant gravitational force (see Fig.11, top right) acting on the particle as it orbits around one quadrant of the ellipse, is drawn to scale at regular intervals in Fig.11(b). We could now take the ratio between  $g_z$  and  $g_x$ , given by equations (2) and (4) respectively, and using the notation  $c = \cos(\phi/2)$ ,  $s = \sin(\phi/2)$  and  $t = \tan(\phi/2)$ , then

$$\begin{aligned} \tan \xi &= \frac{g_z}{g_x} = \frac{\cos \phi}{1 - \sin \phi} = \frac{c^2 - s^2}{1 - 2sc} = \frac{1 - t^2}{1 + t^2 - 2t} = \frac{1 + t}{1 - t} \\ &= \frac{\tan \frac{\pi}{4} + \tan \frac{\phi}{2}}{1 - \tan \frac{\pi}{4} \tan \frac{\phi}{2}} = \tan \left( \frac{\pi}{4} + \frac{\phi}{2} \right) \end{aligned} \quad (25)$$

whence

$$\xi = \frac{\pi}{4} + \frac{\phi}{2} \text{ in radians, or } \xi = 45^\circ + \frac{\phi}{2} \text{ in degrees,} \quad (26)$$

where  $\phi$ , defined in Fig.2, is  $\angle POx$ .

Taking as an example in Fig.11(b) the position of the particle at  $P$ , the line of action of the force acting on the particle cuts the major axis of the ellipse at  $A$ . As the particle  $P$  travels anticlockwise to the pole at the top of the ellipse, point  $A$  travels down the major axis, passes through the focal point, and thence to the pole at the bottom of the ellipse, then it travels back up the major axis. When the particle  $P$  passes through the annular plane, point  $A$  for an infinitesimal instant, becomes coincident with  $O$ , before ‘flipping’ into the upper half of the ellipse where it travels through that focal point in a similar fashion as described.

As a ‘first approximation’ the SGA *does* behave like a point mass at the opposite focus of a semi-ellipse, for any given such orbit, so it is possible to understand why, during our very slow computation of such orbits of such elliptical perfection, that this was the obvious direction in which we would think. The aspect of the mechanics which we found difficult to comprehend is, given that the force on the particle only *approximately* points

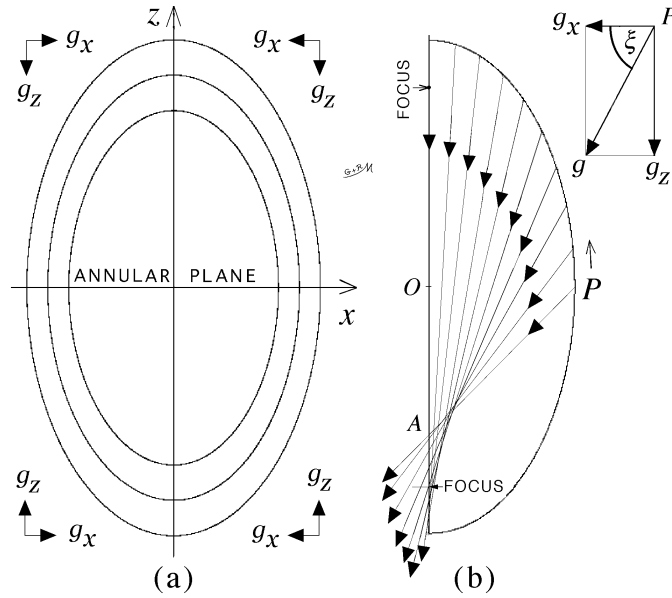


Figure 11: (a) Three ‘ellipses extraordinaires’, each computed in 200,000 steps, giving approximately three circuits per orbit. (b) The force acting on the particle  $P$  systematically wanders from pointing at the focus.

towards the focus on the opposite side, why is the orbital curve apparently so elliptically perfect given how Keplerian mechanics are not being accurately obeyed? We give data shortly on just how accurately elliptical this orbit happens to be.

We found analyzing the mechanics of this orbit very difficult. Unlike Keplerian ellipses, there is no fixed point about which angular momentum is conserved. If  $g_\phi$  given by equation (11) happened to be zero, then equation (10) could yield circular orbits in the polar plane, but with the addition of a force acting outwardly towards the annular rim, these orbits are drawn into ellipses not with their major axis parallel to the annular plane, but perpendicular to it. Of course,  $g_\phi$  rotates towards the annulus as the particle gets nearer to the annular plane, and as it speeds up, the radius of curvature increases, giving an elliptical orbit with major axis perpendicular to the annular plane. After many pages of equations, we still have the feeling, “but we hardly got started!” We watched the Fourier components of the motion of such an orbit behaving very differently compared to a Keplerian orbit of the same eccentricity. This elliptical orbit possesses a very deceptive ‘Keplerian appearance’ and, masquerading as an ordinary orbit, it certainly fooled us into searching by various means for an equivalent mass of the SGA acting at the focus of the orbiting particle, on the opposite side of the annulus. Only after considerable computer and mathematical struggles did we ourselves become used to the idea, “really there’s nothing there, no equivalent static mass exists at either focus of this elliptical orbit”. So that’s why we called this orbit the ‘ellipse extraordinaire’, but the story does

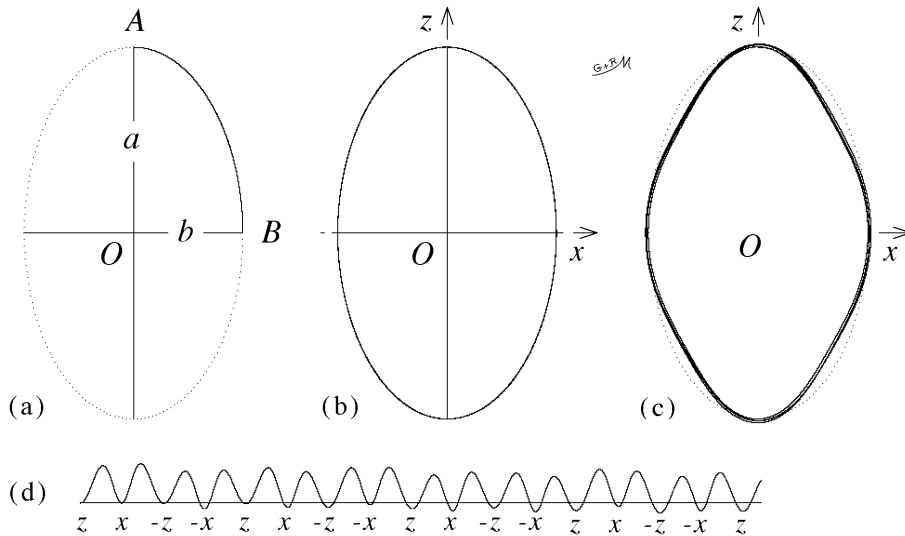


Figure 12: (a) A quadrant of computed orbit is used to construct the rest of a ‘true ellipse’, marked by very fine dots in (a), (b) and (c). In (b) these dots vanish beneath the continuing orbit. (c) gives the difference of radius, magnification  $\times 20$ , between the orbit and the ‘true ellipse’, using the ‘true ellipse’, as a reference. In (d) this inward distortion, magnified  $\times 50$ , is plotted upwardly versus the number of computational steps.

not end here.

If these orbits could be demonstrated by our computing to be geometrically precise, then this would suggest that the differential equations of motion (24), might be solvable, so we investigated their perfection. In Fig.12(a), a quadrant of the computed orbital ellipse is plotted from  $A$  to  $B$ , launching from a point on the  $z$ -axis with  $v_x = 0.579$ . The  $z$ -value at launch point  $A$  is the semi-major axis length  $a (=400)$  of this orbit, and where it crosses the  $x$ -axis at point  $B$ , gives  $b (=235.721)$ , the semi-minor axis length. A ‘true ellipse’, based on these values of  $a$  and  $b$ , was immediately plotted in dotted form in Figs.12(a), (b), and (c). In (b), this ‘true ellipse’ has vanished beneath the continuing plotted orbit, such is its pictorial elliptical accuracy. While this plot is taking place, the length of the radius vector to the orbital ellipse, projected to meet the ‘true ellipse’, is computed and found to be very slightly shorter in the diagonal directions. The difference in radius, magnified 20 times, is then plotted inwardly from the ‘true ellipse’ in (c), showing how it changes around the orbit. A slight quadrature distortion of less than 0.5% decrease in radius in the diagonal directions became apparent. The distortion, magnified 50 times, is plotted versus the number of computing steps in Fig.12(d), where the decrease in radius appears as one peak per quadrant. This slight distortion, not attributable to inaccuracies in our computations, spells trouble for those attempting to solve the simultaneous equations of motion (24), suggesting the existence of small higher order terms in a series type solution, which those skilled in dealing with differential

equations may be able to reveal. But as far as we know, since we have not yet managed to solve them manually, this is a difficult mathematical problem. We present it here as a challenge to readers and quite close to the quatercentenary of the publication of Kepler's *Astronomia Nova* of 1609, containing the book *De Motibus Stellae Martis*, wherein it is deduced that the planets move in ellipses, of which the Sun forms a focus [5].

Before moving to the very interesting 'centre target' orbits in Fig.13, we deal briefly with some of the other orbits seen in our orbital collection, but this is not the full portfolio of strange-looking orbits.

**13.4 'Crab' orbits** (Fig.13): launched perpendicularly from points on the  $z$ -axis with  $v_x = 1.2$ , there is room to show only two such orbits. This orbit is a more complicated variation of the 'St.Louis Gateway Arch' orbit.

**13.5 'Needle and thread' orbit** (Fig.13): launched from  $x = 200$ ,  $z = 50$ , with velocity  $v_x = 1.83$  and  $v_z = -0.4$ , this orbit, found by chance when searching for 'the typical chaotic orbit' for this article, contains two 'instantaneous static points'. One ISP is more stable than the other, giving the appearance of an accurate needle point. The slight wanderings of the other ISP give the appearance of the frayed end of a length of thread.

**13.6 'Goldfish' orbits** (Fig.13): launch parameters,  $v_z = 1.077$ ,  $z = 0$ ,  $v_x = 0$ , from points on the  $x$ -axis, each orbit contains two ISP.

**13.7 'Alpha' orbit** (Fig.13): the particle is released from rest along a radius vector with  $\phi = 12.2^\circ$ .

**13.8 'Propeller' orbit** (Fig.13): this is one launch only of a five-lobe 'propeller' orbit, launched perpendicularly from point  $z = 20$  on the  $z$ -axis with  $v_x$  near to 2.555 and halving the plotting scale to keep the orbit on-screen. By fine adjustment of the launch velocity, the orbiting particle passes through the annular plane several times per cycle, but after two cycles, numerical problems associated with passing near  $O$  herald the onset of small errors followed by chaos. Improving the accuracy of such orbits or searching for more lobes, involves a great deal of computing time.

**13.9 'Centre target' orbits** (Fig.13) **with further analysis and discussion:** in this figure, each orbit is launched from the  $z$ -axis perpendicularly with  $v_x$  set to unity. After launch, each particle heads outwards, passes through the annular plane, then turns and races towards  $O$ . We suspected that a mathematical reason may exist for a particle to pass exactly through  $O$  when launched precisely with unit velocity perpendicularly from the  $z$ -axis, so we investigated this in more detail as follows:-

In Fig.14(a) on page 28, the launch velocity is stepped from 0.95 to 1.05, for within this range the orbit flips from passing  $O$  on one side to passing it on the other, whence this narrows the required launch velocity to between 0.98 and 0.99. This procedure,

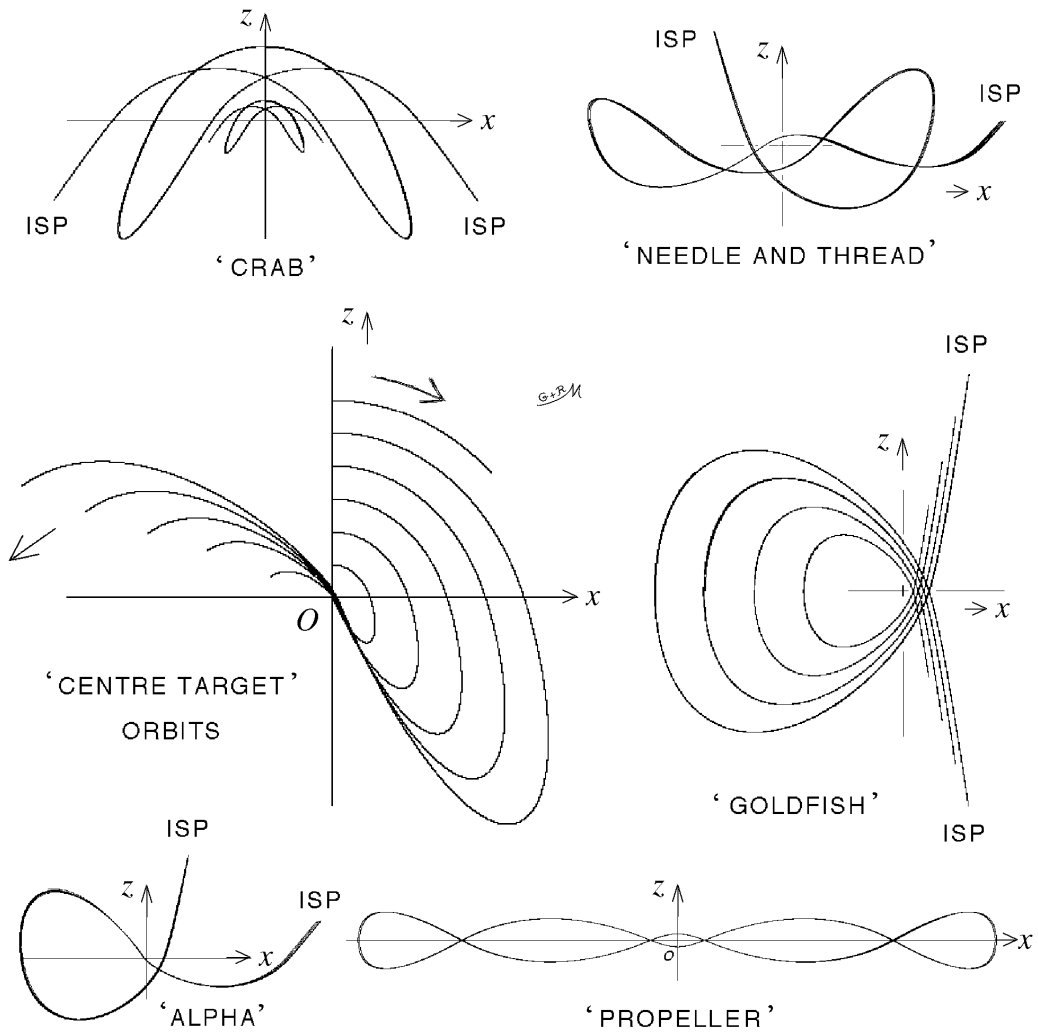


Figure 13: More examples of polar orbits, continued from Fig.9 (page 20).

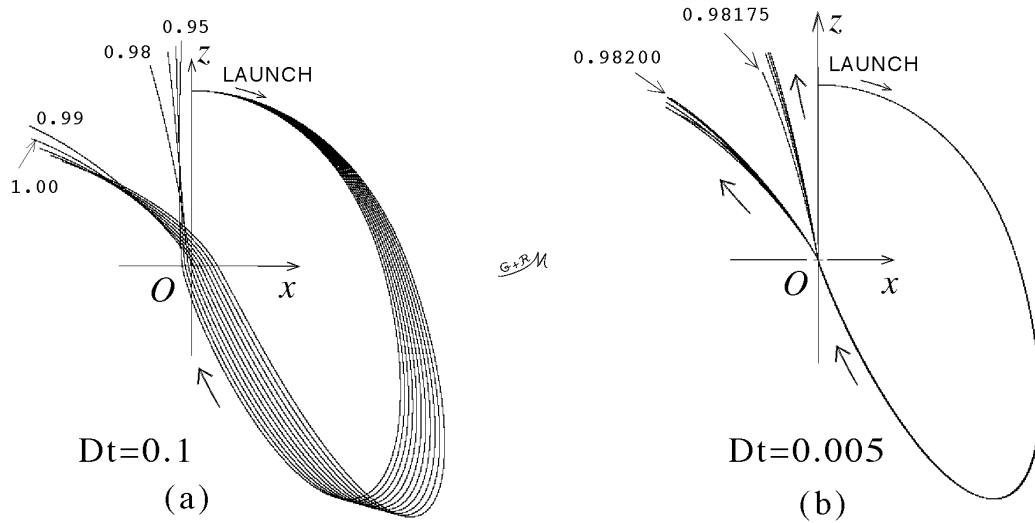


Figure 14: (a) Testing the effect of slightly different launch velocities to find the velocity giving the closest approach to  $O$ . Fine tuning in (b) narrows the launch velocity to between 0.98175 and 0.98200 in normalised units.

repeated in smaller steps, with a reduction of  $Dt$  from 0.1 to 0.005 leads, after several such procedures and diagrams, to the last diagram given in Fig.14(b). This narrowed the limits on launch velocity to between 0.98175 and 0.98200. The process can obviously be continued, but increasing the accuracy demands running the program for longer.

In theory, with Newtonian mechanics applying, a particle travelling towards the very centre of the SGA, is set on a journey of ever increasing speed. But as the speed increases, the slightest error off-target would cause the particle to deviate and, after the close encounter, to come flying out with great speed, slowing in a reversible fashion since the gravitational force field is conservative. However, if it be imagined that a particle really can travel into the centre, this journey of ever increasing speed and ever decreasing potential energy, appears to invoke no theoretical reason why the particle should ever re-emerge. Disappearance of the particle in such a manner would signal an irreversibility in the mechanics of the SGA, caused by a singularity in the area mass density. Hence when a particle is seen to re-emerge after an encounter with the centre, during computing, this suggests that the very centre has been missed. Physically, of course, this is very interesting, for since closer proximity to the centre is associated with increasing attraction, it might be expected to be a very easy target, but on the contrary, it is very difficult, if not impossible, to hit the target precisely. What happens during computing, as in Fig.14(b), has its similarities to diffraction.

A simpler problem can be studied in one dimension by launching a particle directly towards  $O$  along the  $x$ -axis, at the same time it would interesting to see if numerical errors cause the computed orbit to turn back into a two-dimensional one. Using this

launch condition, we see the computational errors get larger as the speed increases and the updated positions of the particle become spaced by bigger distances, until the particle erroneously skips across  $O$ , sometimes several times, suddenly becoming ejected at huge speed in either the positive or negative direction. This is entirely a computing problem but at least it remained purely a one-dimensional situation. Given the isomorphism of the orbits of an SGA, reducing  $Dt$  to improve accuracy never ultimately succeeds, because the picture can always be magnified, whereupon exactly the same kinds of error can be seen yet again, however much  $Dt$  be reduced.

The mass  $M(r)$  of that part of an SGA, contained within a circle of radius  $r$  on the annular plane centred on  $O$ , is given, using a substitution from equation (1), by

$$M(r) = \int_0^r 2\pi r \sigma dr = 2\pi \int_0^r k dr = 2\pi kr \quad (r > 0), \quad (27)$$

so this mass is proportional to the radius of the enclosing circle. As this radius is reduced, the enclosed mass also reduces and tends to zero, so the singularity at the centre of the SGA appears to be different from a black hole.

**13.10 ‘Circular string-mat’ orbit** (Fig.15(a)): the particle is released from rest at a point with co-ordinates  $(20, 0, 400)$  giving a chaotic orbit in the  $x, z$  plane, whence the particle is seen to have approximately the same apogee range from the centre in any direction, making a circular mat shape. If an attempt be made to convert this orbit into a three-dimensional ball by giving the orbit some angular momentum around the  $z$ -axis, then this takes us to the next section,

## 14. Non-planar orbits

Before discussing the computing, we immediately continue from above by discussing what happens when the two-dimensional ‘circular string-mat’ orbit seen in Fig.15(a) is given angular momentum around the  $z$ -axis, as follows.

**14.1. ‘Ball of string’ orbit** (Fig.15(b) through (e)): Fig.15(a) was obtained by releasing a particle from rest from vector position  $(20, 0, 400)$ , but if the particle be launched with vector velocity  $(0, 0.1, 0)$ , from the same launch position, then this gives the particle a small angular momentum around the  $z$ -axis. The orbit looks much the same when seen in the side-view projection in (b), but in plan view (looking down the  $z$ -axis) in (c) a star pattern forms, illustrating the fun of watching orbits live on-screen. (Some of them are ‘only obvious with hindsight’.) The major lobes of this tangled orbit are very planar, with the greatest changes in direction occurring when the particle is close to the  $z$ -axis. This has similarities to the well-known ice-skating spin analogy—arms stretched out slows the rotation, arms drawn in quickens the spin—but to explain the stellate appearance of the orbits seen in (c), this analogy needs pushing to an extreme: practically all the rotation takes place when the particle is very close to the  $z$ -axis, and scarcely any rotation occurs when the particle is orbiting further away. Of course, we wished to see what happens when the particle is launched with greater angular momentum, so

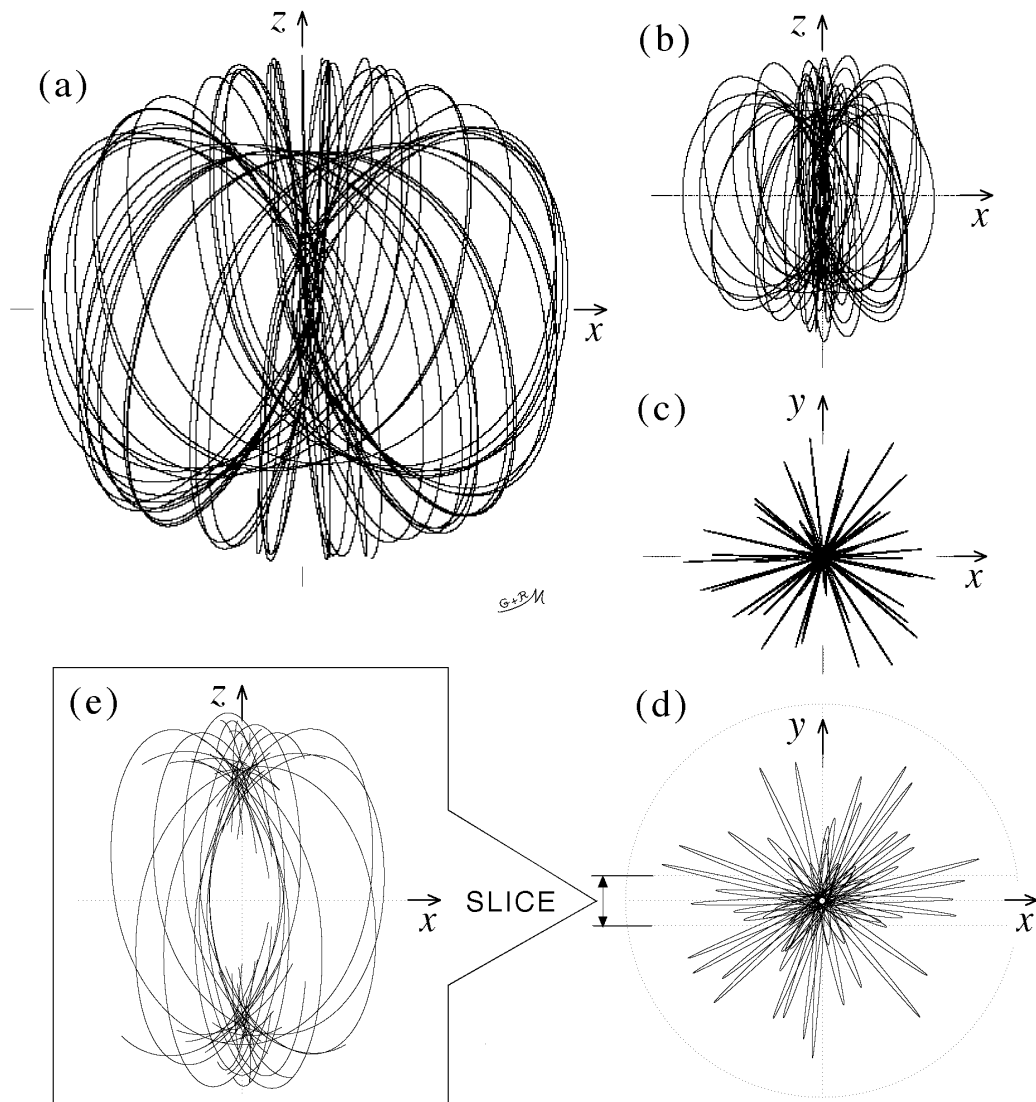


Figure 15: (a) ‘Circular string-mat’ orbit in the polar plane, and in (b) this orbit is given a slight angular momentum around the  $z$ -axis so becoming a three-dimensional ‘ball of string’ orbit. Viewed in plan in (c) the particle performs approximately planar orbital lobes, changing direction when the particle nears the  $z$ -axis. (d) The orbit is launched with a greater angular momentum around the  $z$ -axis, a slice parallel to the  $x,z$  plane, viewed in (e), shows that a central hole has developed.

the consequences of increasing the launch velocity  $v_y$  to 0.3 are seen in Fig.15(d) and (e). A similar stellate effect is seen in the plan view in (d), the slightly increased tilt of the major lobes, seen very glancingly when viewed down the  $z$ -axis, opens the ‘points of the star’ seen in (c), into apparently very narrow loops in (d). Suspecting that the ‘string ball’ had become hollow, we cut a thick slice through it, seen in section in (e), and confirmed this feature.

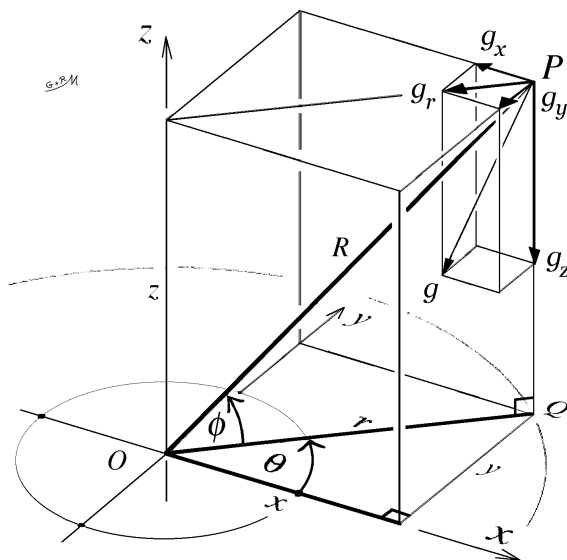


Figure 16: Three-dimensional geometry.

respectively, with  $\theta$  measured in the  $x,y$  plane, likewise  $r$ , both being specified in Fig.16, where

$$r = \sqrt{x^2 + y^2} \quad (31)$$

and

$$R = \sqrt{x^2 + y^2 + z^2}. \quad (32)$$

Equation (20) *viz.*  $g_z = 1/R$ , still applies, using equation (32) for  $R$ . Values of  $\sin \theta$  and  $\cos \theta$  can be obtained directly from distance ratios without calculating the angle. Other details of three-dimensional orbit computing are given in Section 10.

**14.3 ‘Daisy’ orbits** (Fig.17): One such orbit is shown in elevation, plan and isometric view in Fig.17(a), (b) and (c) respectively. This orbit is obtained by giving the ‘St.Louis Gateway Arch’ orbit (see Section 13.2, page 19) a slight angular momentum around the  $z$ -axis by launching the particle from point  $(200, 0, 130)$  with velocity vector  $(0, 0.1, 0)$ . A stereo-isometric pair of images is given for a simpler such orbit, in Fig.17(d) and (e) respectively, the two images being computed by rotating a pair of isometric projections oppositely through small angles ( $1.5^\circ$ ) around the  $z$ -axis.

#### 14.2. Computing orbits in three dimensions:

The gravitation  $g$  at point  $P$  with coordinates  $(x, y, z)$  resolves into  $g_z$  and  $g_r$ , where  $g_r$ , the radial component of gravitation parallel to the annular plane (note: this is not  $g_R$ ), is obtained from equation (21) (page 13) which, with the same restrictions on  $\phi$  and  $R$ , becomes

$$g_r = \frac{1}{R} \left( \frac{1 - \sin \phi}{\cos \phi} \right), \quad (28)$$

and  $g_r$  resolves into the respective Cartesian components  $g_x$  and  $g_y$  given by

$$g_x = g_r \cos \theta = g_r \frac{x}{r} \quad (29)$$

and

$$g_y = g_r \sin \theta = g_r \frac{y}{r} \quad (30)$$

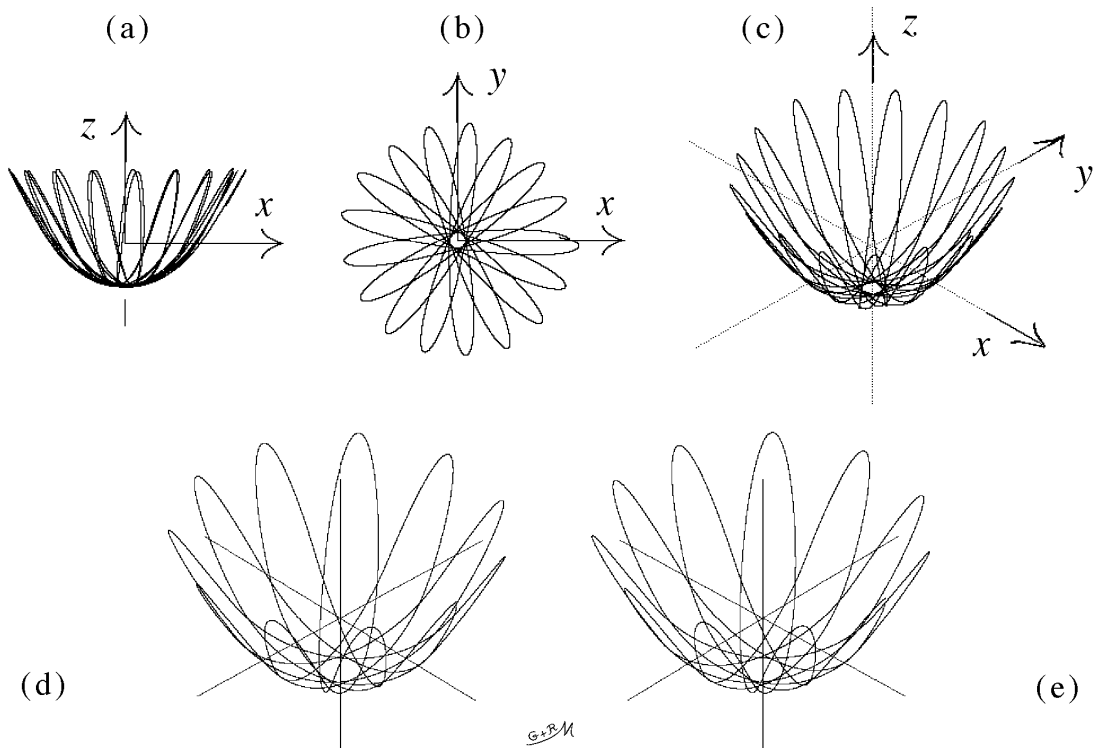


Figure 17: ‘Daisy’ orbit seen in (a) elevation, (b) plan view, and (c) isometric view. (d) and (e) are stereo-isometric views of a simpler daisy orbit.

**14.4 Annular oscillatory orbits** (Fig.18, page 33): Oort discussed and analyzed the motions of stars moving up and down in a direction parallel to the  $z$ -axis of the Milky Way [6]. The SGA readily exhibits such orbits. The frequencies of oscillation are very amplitude-dependent for an SGA, and the vertical scale was expanded 60 times so that orbits of low amplitude and high oscillation frequency could be seen. Each orbit is obtained by launching a particle in the  $x,y$  annular plane, at various radii, with a circumferential speed of unity, adding a small  $z$ -component of velocity at launch, kept constant for the isomorphic family of such orbits in this diagram. In the ‘Preview picture’ where the scales are equal along each axial direction, the amplitude of the oscillations is considerably greater so the oscillation frequencies are less in that picture. The strong dependence of frequency upon the amplitude arises from the mathematically sudden change to the opposite direction of  $g_z$  as the particle passes through the annular plane of the SGA. In reality, this change cannot take place so fast, so less dependence of frequency upon amplitude within an annular layer of finite thickness is to be expected.

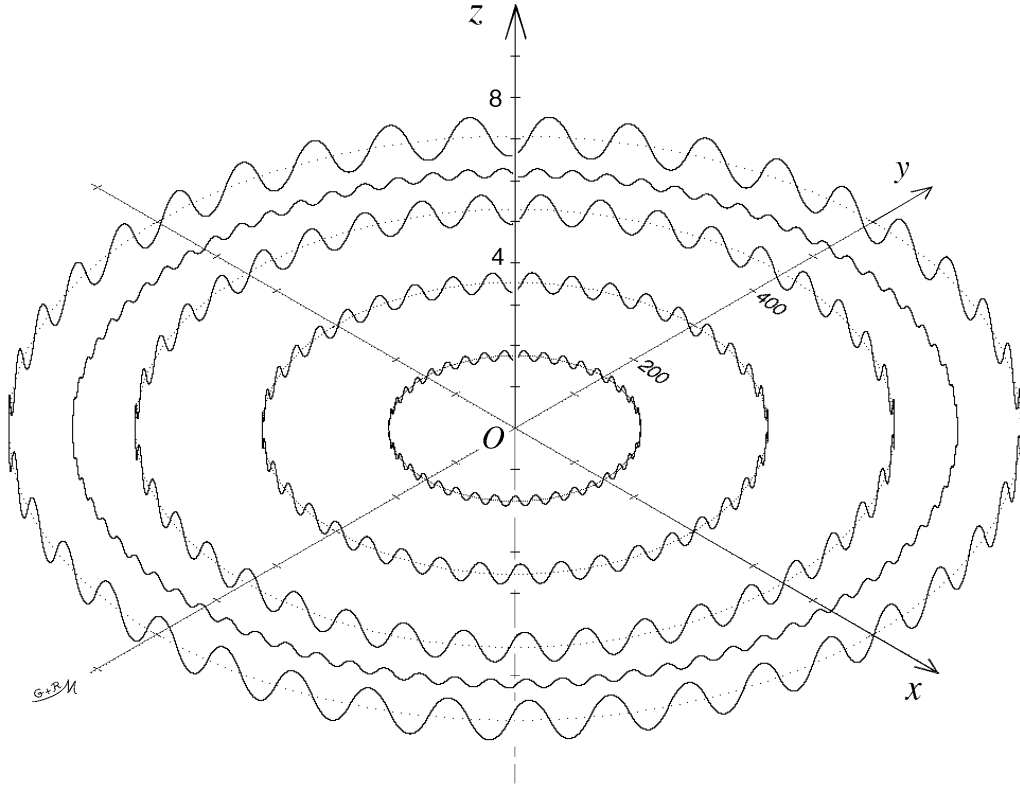


Figure 18: Annular oscillatory orbits seen in isometric view. The vertical scale is magnified 60 times to enable ‘high frequency’ low amplitude oscillations to be seen. The isomorphic orbital family launch parameters are  $v_x = \frac{-1}{\sqrt{2}}$ ,  $v_y = \frac{+1}{\sqrt{2}}$ ,  $v_z = 0.04$  and  $x = \frac{-a}{\sqrt{2}}$ ,  $y = \frac{-a}{\sqrt{2}}$  and  $z = 0$  where  $a = 150, 300, 450,$  and  $600$  units, respectively. For the single small amplitude orbit of large radius,  $a = 525$  and the launch velocity  $v_z = 0.02$ , *i.e.* half that of the isomorphic family.

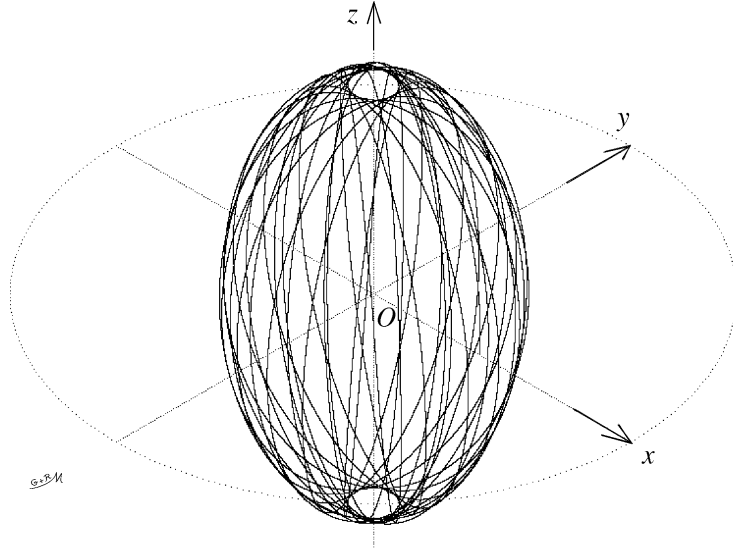


Figure 19: A single rotating polar elliptical orbit generates a ‘rugger ball shape’ in three dimensions, seen in isometric view, the particle is launched from point  $(250, 0, 0)$  with vector velocity  $(0, 0.1, 5/3)$ .

**14.5 Rotating polar elliptical orbit** (Fig.19): launched from point  $(250, 0, 0)$  with vector velocity  $(0, 0.1, 5/3)$ , this orbit reminded us of the various pictures of spiral galaxies exhibiting polar orbits described by Rubin [7]. Given all the various types of computed polar orbit seen in Figs.9 and 13, perhaps in reality some physical characteristic particularly favours the formation of polar elliptical orbits instead of the various other types. For example, elliptical orbits might have the greatest stability because particles in such orbits can stay away from the centre for many cycles, and such orbits cut the annulus perpendicularly so encountering the least amount of annular material. But we notice in our computing that elliptical polar orbits can sustain a wide variation in launch conditions whilst still remaining approximately elliptical. Although wandering in position and angle, these approximately elliptical orbits show little tendency to turn into some other form of orbit. This is illustrated in Fig.20, where the same scale applies to each plotted orbit and the particle is launched in the polar plane from the same position on the  $x$ -axis, shown in the middle of the picture. The number identifying each orbital picture is the vertical launch velocity used in each computation, covering the velocity range from 1.5 to 2.2, whereupon a propensity to form elliptical orbits is evident. ‘Ellipses extraordinaires’ are orbits with their launch velocity accurately adjusted to cause the orbits to retrace themselves as exactly as possible, closest to 1.7 in Fig.20, giving the narrowest band of wandering orbits. Other repeating orbits which involve a particle passing at glancing angles through the annulus are more likely to interact with the matter of the annulus in a real galactic situation. The ‘propeller’ orbit of Fig.13, for example, has so many

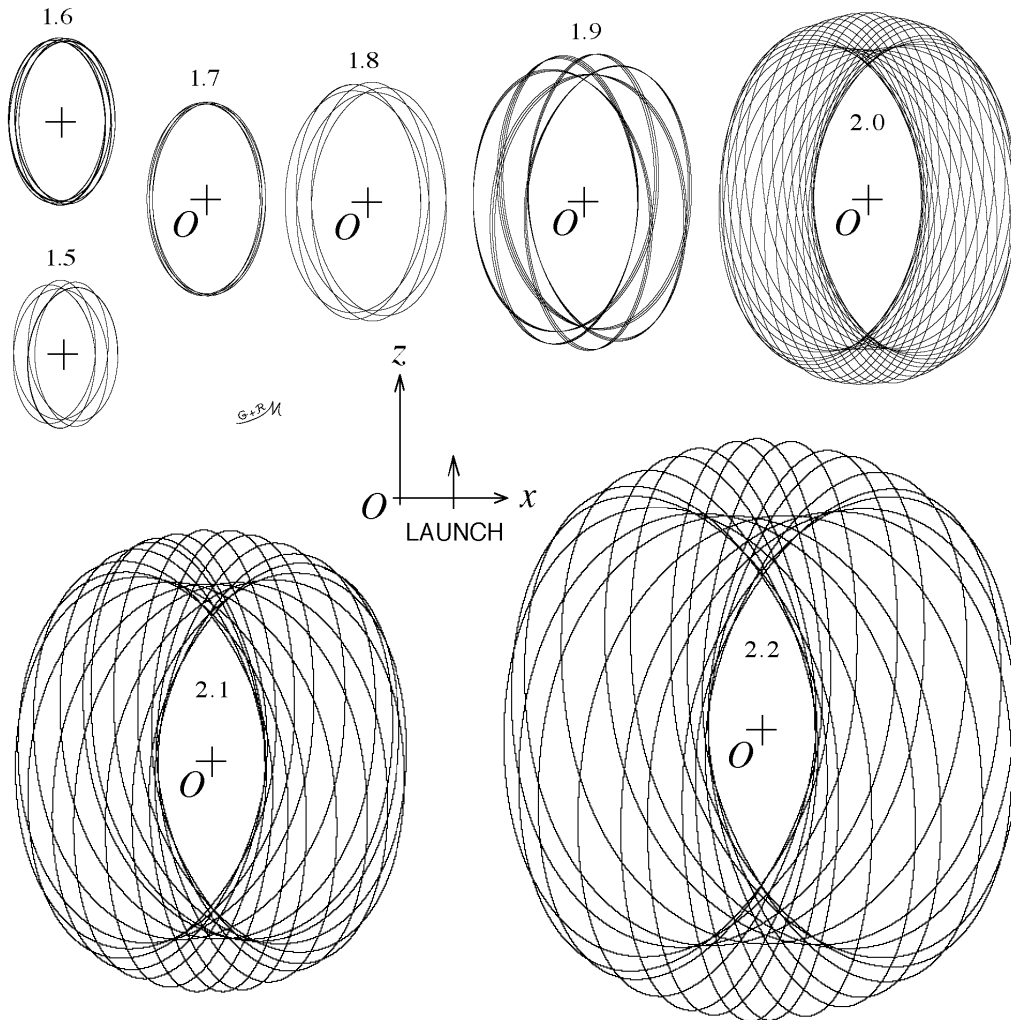


Figure 20: Planar polar orbits executed by a particle launched perpendicularly from the same point ( $x = 200$ ) on the  $x$ -axis, with a velocity ranging from 1.5 to 2.2 normalized units.

annular interactions, that we think it would be unlikely to occur in reality, moreover, what happens in the centre of a galaxy is rather different from an SGA. Perhaps the polar orbit most likely to survive for the longest time is when a particle is thrown out with sufficient speed perpendicularly from the annulus, whence it is free to execute an orbit like those of Fig.20 at least for half a cycle.

## 15. Brief further discussion

The flat rotation curves of spiral galaxies, described by Rubin [7], start off from near zero at the centres of such galaxies, so they differ, particularly at small radii, from the flat rotation curve of the SGA which has a constant circular rotation speed following equation (7), which still applies as the radius tends to zero. (A ‘rotation curve’ is a plot of circular orbit speed versus radius, in the plane of a spiral galaxy.) Before arriving at our very mathematical SGA, we had been modelling spiral galaxies by combining the gravitational effects of a spherical nucleus that fitted geometrically into the hole of an annulus and experimented with various tapering area mass densities as a function of radius for the annulus. We used the algorithm of Stage 4(a), Section 10, particularly to obtain radial gravitation in the annular plane without requiring orbital computations at that time. This kind of model has a ‘rotation curve’ that starts at the origin and the more constant the curve becomes, the more closely is the model producing radial gravity  $g_r$  that falls inversely with the radius  $r$  (because  $V_{rot} = \sqrt{rg_r}$ ). Beyond the boundary of the spherical nucleus, the gravitation caused by the nucleus, which decreases according to the inverse square law, can be ‘boosted’ by annular gravitation. But eventually we found that at large distances from the nucleus in our modelling, the gravitation from the annulus can become the dominant contributor because however masses may be distributed at or near to the centre of the model in the nucleus, their gravitational effects, or lack of them if the centre be left empty, has insignificant effect upon the distant gravitational field compared to the contribution made by an annulus such as one that starts at a finite radius near to the centre, and thereafter decreases in area mass density in inverse proportion to the radius. This applies to gravitation not only in the annular plane, but also at large angles away from the annular plane as far as the  $z$ -axis. Removing material from the centre of an SGA does not alleviate the problem of the depth of this very wide potential well, which in theory remains infinitely deep, on account of the very thin matter in the outer reaches of the annulus, as it extends mathematically to infinite radius. When doing all these computational experiments, which we encourage, it will be noticed that the gravitation within the central hole of an annulus is radially outwards, so no circular orbits are possible within this hole until enough mass has been placed, for example, at the centre, or distributed as a uniform sphere, to counteract the outward acting gravity caused by the annulus. If the outer region of an SGA be truncated beyond a certain radius, the velocity rotation curve rises towards the edge of the remaining annulus because the removal of the outer portion increases the radial gravitation towards the edge of what remains.

Just in case this is the first time that the reader has studied this subject, we emphasize here that our gravitational equations for the SGA have been derived by the

application of Newton's inverse square law of gravitation to this particular mass distribution, which we call a 'special gravitating annulus', and it has the characteristic of producing a gravitational field that falls inversely with the radius, not radius squared [1]. This gravitational field is amenable to simple mathematics in three dimensions without running into the problems of elliptic functions. The SGA is also amenable to the computation of some remarkable orbits, and to basic mechanical considerations of what happens in the very middle with respect to Newtonian gravitation. Some fairly deep mathematical research needs to be done to understand the 'ellipse extraordinaire', the 'St.Louis Gateway Arch' and the various other orbits. We think that this qualifies this annulus as being really rather special.

## 16. Appendix: Justification for the assumption of the area mass density varying inversely with the radius.

Our mathematical analysis of the SGA given in reference [1], cited near to the beginning of the present article, began with the assumption of the particular mass distribution given by equation (1). We justify this as follows. (Note: in this Appendix, subscripts are needed for radial gravitation  $g_P$  and  $g_Q$  at points  $P$  and  $Q$  respectively, so the symbol 'g' is used here for the radial gravitation in the annular plane and here the constant  $k$  of equation (1) appears as ' $k_1$ ' to distinguish it from another constant  $k_2$  that appears shortly.) We start by assuming that a self-gravitating plane annulus is mathematically possible, where the radial gravity  $g$  in the annular plane at radius  $r$  is given by

$$g = \frac{k_1}{r} \quad (r > 0) \quad (A.1)$$

where  $k_1$  is a constant (equal to the square of the circular orbit speed). By the application of Newton's law of gravitation, we then attempt, using mathematical reasoning, to find a function  $\sigma(r)$ , if such a function exists, for the area mass density  $\sigma$  at radius  $r$ .

In Fig.21,  $O$  is the centre of the annulus and the plane of the paper is the annular plane. Any fixed point  $P$  is chosen in the annular plane at radius  $R_P$  where  $R_P > 0$ . On  $OP$  projected is another point  $Q$ , at radius  $R_Q$ , given by

$$R_Q = \beta R_P \quad (\beta > 0, \beta \neq 1) \quad (A.2)$$

where  $\beta$  is the 'scaling factor', maintained constant for the time being. For every  $n^{\text{th}}$  infinitesimal area element  $\delta A_{P,n}$  at a distance  $p_n$  from  $P$  and an angle  $\theta_n$  with respect to  $OP$ , there is a corresponding  $n^{\text{th}}$  infinitesimal area element  $\delta A_{Q,n}$  of the same shape but scaled up in size at a distance  $q_n$  from  $Q$ , and at an angle  $\theta_n$  with respect to  $OQ$ . The elements are located along a radius at respective distances  $r_{P,n}$  and  $r_{Q,n}$  from  $O$ . Various equations apply due to the scaling, these are:

$$r_{Q,n} = \beta r_{P,n} \quad (A.3)$$

$$q_n = \beta p_n \quad (A.4)$$

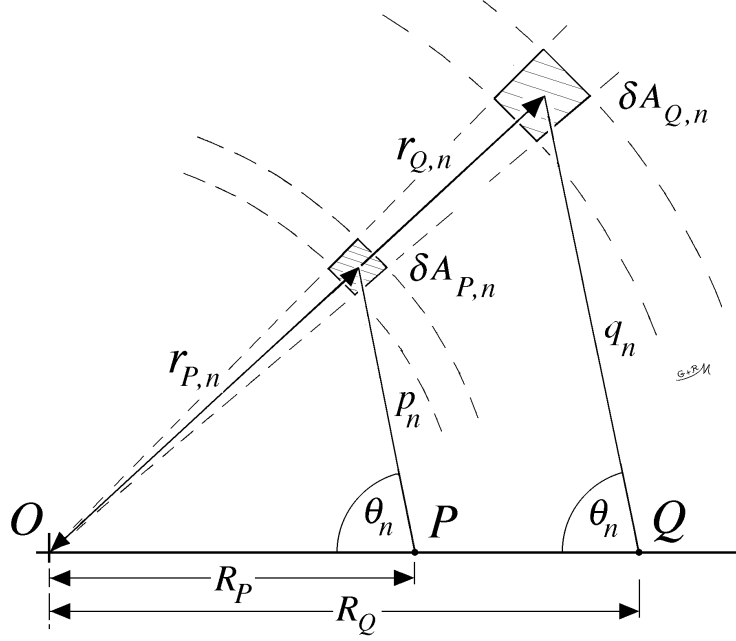


Figure 21: The  $n^{\text{th}}$  pair of elemental areas are chosen on the annular plane, which is the plane of this diagram.

and

$$\delta A_{Q,n} = \beta^2 \delta A_{P,n} . \quad (\text{A.5})$$

Applying Newton's law of gravitation (with the gravitational constant set to unity) then the total radial gravitational component  $g_P$  towards  $O$ , at point  $P$ , is given by equation (A.6) as follows, the summation being performed over the entire annulus, the elemental areas being of a shape to tessellate the plane,

$$g_P = \frac{k_1}{R_P} = \sum_{n=1}^{\infty} \sigma(r_{P,n}) \frac{\delta A_{P,n}}{p_n^2} \cos \theta_n . \quad (\text{A.6})$$

Similarly the total radial gravitational component  $g_Q$  towards  $O$ , at point  $Q$ , is given by equation (A.7) as follows

$$g_Q = \frac{k_1}{R_Q} = \sum_{n=1}^{\infty} \sigma(r_{Q,n}) \frac{\delta A_{Q,n}}{q_n^2} \cos \theta_n . \quad (\text{A.7})$$

By rearranging equations (A.6) and (A.7), and using substitutions from equations (A.2), (A.3), (A.4) and (A.5), two expressions for  $k_1$  are obtained which, when placed equal

to each other, yield:

$$\sum_{n=1}^{\infty} \sigma(r_{P,n}) \frac{\delta A_{P,n}}{p_n^2} \cos \theta_n = \beta \sum_{n=1}^{\infty} \sigma(\beta r_{P,n}) \frac{\delta A_{P,n}}{p_n^2} \cos \theta_n . \quad (\text{A.8})$$

This equation can be balanced by equating the  $n^{\text{th}}$  term on each side, so then

$$\sigma(r_{P,n}) = \beta \sigma(\beta r_{P,n}) . \quad (\text{A.9})$$

This equality holds independently of  $\beta$  provided that the function  $\sigma(r)$  is given by

$$\sigma = \frac{k_2}{r} \quad (r > 0) \quad (\text{A.10})$$

where  $k_2$  is another constant.

It might appear that other ways to balance equation (A.8) may exist, yielding alternative solutions for  $\sigma(r)$  but Poisson's equation indicates that as soon as a particular mass distribution is specified, such as equation (A.10), then, with no external influences, this fixes the gravitational field in three dimensions around the annulus. This means that if any other solution existed conforming with equation (A.1) for radial gravitation in the annular plane, but which had a mass distribution different from equation (A.10), then this would require a different gravitational field component perpendicular to the annulus, above and below the annular plane. But since the latter field is generated by the mass distribution of the annulus itself without external influences, then it follows that equation (A.10) is the only exact solution, thus justifying equation (1) both at the start of the present article, and at the start of reference [1].

Whilst our method does not yield the value of the constant  $k_2$  in terms of  $k_1$ , a particular physical aspect of this annulus became very apparent: the radial gravitation  $g$  at a point  $P$  is directly proportional to the mass density  $\sigma$  at that point and is given by

$$g = \frac{k_1}{k_2} \sigma \quad (\text{A.11})$$

obtained from equations (A.1) and (A.10). We are unsure exactly what the physical significance of this is, but when attempting to get to the above solution for  $\sigma(r)$ , this particular feature of this annulus struck us as very remarkable, for despite the gravitation at any point on the annulus being caused by the matter of the total annulus, somehow it sums to give a local value of gravitation that is directly proportional to the local area mass density for any point on the annulus (apart from the origin). If that is what tends to happen in the outer regions of spiral galaxies (which exhibit 'flat rotation curves' [7]), then the question becomes, what is the physical process that causes this to happen? We have added this to our list of interesting things to study.

Guy Moore & Richard Moore  
November 2010

## 17. References and Notes

- [1]. ‘A special gravitating annulus’ Guy Moore and Richard Moore, *Mathematical Gazette* vol.93, No.527, July 2009, pp.347-352.
- [2]. This appears to cause difficulties when attempting to find out how much a ray of light would be deflected by gravitation when emitted, for example, perpendicularly from a point on the SGA—the only such problem we have briefly examined so far. The deflections appear to be large enough to violate small angle approximations.
- [3]. Pictures of the St.Louis Gateway Arch can be seen on:  
[www.gatewayarch.com/Arch/info/act.riverboat.aspx](http://www.gatewayarch.com/Arch/info/act.riverboat.aspx).  
The arch provides a fascinating match to these particular orbits seen in the ‘Preview picture’ and in Fig.9 (page 20).
- [4]. Some of our work is discussed in ‘The art of spiral galaxy computing: a rich area for amateur astronomers’ Guy Moore, *New Zenith, The Monthly Magazine of the Vectis Astronomical Society* vol.15, No.5. June 2007, p.7, and in accompanying issues.
- [5]. ‘Kepler, Johann’, *The Oracle Encyclopaedia* R.W.Egerton Eastwick, Newnes, London, 1895, vol.3, p.569.
- [6]. ‘The force exerted by the stellar system in the direction perpendicular to the galactic plane and some related problems’ J.H.Oort, *Bulletin of the Astronomical Institutes of the Netherlands* vol.VI, No.238, 1932, pp.249-287.
- [7]. *Bright Galaxies, Dark Matters* Vera Rubin, AIP Press, Springer-Verlag, New York, 1996, particularly the sections ‘SO Galaxies with Polar Rings’, pp.54-58, and ‘Dark Halos around Spiral Galaxies’ pp.119-121. Many examples of rotation curves are given, such as on p.52, p.110 and p.136. This book must not only be valued for its wealth of data and discussion, but also for its inspiration, we particularly like ‘Where in the World Is Berkeley, California?’ pp.214-219.

## 18. Acknowledgements

We express our thanks to the helpful staff of the Isle of Wight Council Libraries and for the use of the Internet facilities, and we express our thanks to Wolfram Research Inc. for the use of the Wolfram Integrator, a wonderful mathematical facility accessible in our Public Libraries.